Mon. Not. R. Astron. Soc. **350,** 1087–1106 (2004) doi:10.1111/j.1365-2966.2004.07720.x

Structural parameters of nearby emission-line galaxies

Miguel Sánchez-Portal,[1⋆] Ángeles I. Díaz,[2] Elena Terlevich[3]† and Roberto Terlevich[3,4]

[1] *Universidad Pontificia de Salamanca en Madrid, Paseo de Juan XXIII 3, 28040 Madrid, Spain*
[2] *Department de Física Teórica, C-XI, Universidad Autónoma de Madrid, Cantoblanco, 28049 Madrid, Spain*
[3] *Instituto Nacional de Astrofísica, óptica y Electrónica, Tonantzintla, Puebla, México*
[4] *Institute of Astronomy, Madingley Road, Cambridge CB3 0HA*

Accepted 2004 February 10. Received 2004 February 10; in original form 2003 September 24

ABSTRACT

We present the results of an investigation on the main structural properties derived from *VRI* and Hα surface photometry of galaxies hosting nuclear emission-line regions [including Seyfert 1, Seyfert 2, low-ionization nuclear emission region (LINER) and starburst galaxies] as compared with normal galaxies. Our original sample comprises 22 active galaxies, four starbursts and one normal galaxy and has been extended with several samples obtained from the literature. Bulge and disc parameters, along with the bulge-to-disc luminosity ratio, have been derived applying an iterative procedure. The resulting parameters have been combined with additional data in order to reach a statistically significant sample. We find some differences in the bulge distribution across the different nuclear types that could imply families of bulges with different physical properties. Bulge and disc characteristic colours have been defined and derived for our sample and compared with a control sample of early-type objects. The results suggest that bulge and disc stellar populations are comparable in normal and active galaxies.

Key words: galaxies: active – galaxies: photometry – galaxies: structure.

1 INTRODUCTION

Global active galactic nuclei (AGN) host galaxy properties, including mass, luminosity concentration, morphological type, bulge-to-disc relationship, metal abundance and total luminosity, may influence nuclear activity and perhaps in turn be affected by it. It has been argued that there can exist a connection between nuclear activity and intense star-formation episodes. While there are some observational indications that star formation is enhanced in circumnuclear regions of Seyfert galaxies (see, for instance, Hunt & Giovanardi 1992), other observations point in the opposite sense (e.g. Carone 1992). An outstanding, still controversial question is related to the fuel supply involving the transport of large quantities of mass from reservoirs located in the galactic disc (see, for instance, Shlosman, Begelman & Frank 1989); in this process the matter has to lose almost all of its angular momentum. This can be accomplished by gravitational torques produced by non-axisymmetric perturbations in the gravitational potential. These are associated either with interactions with companion galaxies or with structural features like bars, rings, oval distortions, etc.

Current research on structural properties of galaxies hosting nuclear activity is now largely concentrated in the near-infrared (NIR) bands. There are several advantages in the use of the NIR for studying the host galaxy properties of AGN: on the one hand, a normal stellar population is dominated by old red giants and therefore peaks around 1 μm. On the other, dust extinction is substantially reduced at these wavelengths. Therefore, the NIR is ideal to look for bars and morphological distortions that can be hidden by dust in optical wavelengths (e.g. Mulchaey & Regan 1997). Moreover, the contrast between stellar and non-thermal contributions is maximized, since the latter has a local minimum around 1 μm.

Hunt et al. (1997) performed NIR J, H, K broad-band images and colours in a sample of 26 galaxies with $z \geqslant 0.015$ and found that the average colours, both of the outer and the inner discs, are independent of the activity class and equal to those of normal spiral galaxies. Outer disc colour gradients are also consistent with those of normal spirals. On the other hand, on a scale of a few kiloparsecs from the centre, starburst galaxies show ongoing star formation; in Seyfert 2 galaxies, they found evidence of 'fossil' star-formation activity a few hundred Myr old; finally, no evidence of star formation, either ongoing or fossil, exceeding that of a normal spiral, is found in Seyfert 1 galaxies. They infer an evolutionary starburst–Seyfert connection, although not so global and not so tight in time as previous studies implied. NIR structural parameter analysis from Hunt et al. (1999) shows that bulges of Seyfert and starburst galaxies follow very closely the trend defined by normal spiral bulges and elliptical galaxies. On the other hand, for a given disc effective radius, the mean surface brightness of the Seyfert discs is higher (by $\sim$0.9 K mag arcsec^{-2}) than those of early-type spirals.

⋆E-mail: miguel.sanchez@upsam.net
†Visiting Fellow, Institute of Astronomy, Cambridge.

Márquez et al. (2000) performed NIR J and K' broad-band imaging and colours on nearby, isolated spiral galaxies either with an active nucleus (18 objects, either Seyfert 1 or Seyfert 2 according to Véron-Cetty & Véron 1993) or without it (11 galaxies). They state that global properties are similar in both active and non-active galaxies, since both samples define the same bulge Kormendy relation between the effective magnitude (μ_e) and the effective radius (r_e)[1] and disc components also share the same properties (contradicting the result from Hunt 1999); they also found that bulge and disc scalelengths are correlated, with $r_{\rm bulge} \approx 0.2\, r_{\rm disc}$. On the other hand, NIR central colours of active galaxies are found to be redder than those of non-active spirals, most probably due to the AGN light re-emitted by the hot dust and/or to the presence of active star formation in circumnuclear regions.

In spite of the advantages of the NIR region for such studies, optical wavelengths can still provide useful data. The use of the optical region has its own advantages: on the one hand, observers can benefit from the large size of current optical detectors, providing a convenient sampling of the galaxy disc; on the other, optical studies can rely on the large quantity of published data. Moreover, optical colour maps can be used as excellent tracers of the line-emission regions present in AGN and starburst galaxies (see, for instance, Terlevich et al. 1991)

Early work from Yee (1983) using a SIT-vidicon camera has been followed by a large number of studies using CCD detectors. Mediavilla, Pastoriza & Battaner (1989) and Pastoriza, Mediavilla & Battaner (1989) performed *VI* broad-band surface photometry on a sample of 13 Seyfert galaxies; they consider two classes: 'bulge galaxies' and 'disc galaxies' and found that the $V - I$ colour has a constant, equivalent value in both galaxy groups in the 3-kpc aperture, indicating similar stellar populations, but outside the 5-kpc aperture colours become bluer for disc galaxies and redder for bulge galaxies. Mediavilla et al. (1989) use the same sample to obtain bulge and disc parameters from the surface brightness radial profiles, finding that structural parameters are comparable to those of normal spirals and ellipticals.

MacKenty (1990) performed Kron–Cousins *BVR* CCD surface photometry of 51 Seyfert galaxies from the NGC and Markarian catalogues, finding that in almost all cases, a mechanism to transport material to the nucleus is present (either bars or interactions); about one-fifth of the sample is composed of amorphous galaxies; some of them may be a remnant of past interactions. Colours and disc morphological parameters are in general similar to those found in normal spiral galaxies.

Xanthopoulos (1996) performed *VRI* CCD surface photometry of 27 Seyfert galaxies belonging to types 1 and 2, and intermediate categories, finding that:

(i) generally, Seyfert galaxies are perturbed objects (either by bars or by interactions);

(ii) nearly half of the sample galaxies are barred; moreover, almost all of them present evidence of the existence of a mechanism to transfer material to the nuclear region;

(iii) all non-barred galaxies are either S0 or Sa;

(iv) Seyfert 1 and Seyfert 2 galaxies follow a very similar Hubble-type distribution; Seyfert 2 galaxies tend to have redder nuclei;

(v) Seyfert 1 and Seyfert 2 galaxies present the same disc colours;

(vi) colour gradients remain constant along both the bulge and the disc of the galaxy for both Seyfert types;

(vii) both types of Seyfert galaxy show the same range and dispersion of bulge and disc morphological parameters, and also similar bulge-to-disc luminosity ratios; the wide range of scalelengths observed in Seyfert galaxies may support their classification as early-type spirals. Moreover, the bulge and disc parameters of both Seyfert types are the same as those of normal early-type spirals.

Virani, De Robertis & VanDalfsen (2000) performed R surface photometry on a sample of 32 Seyfert and 45 non-active galaxies[2] from the CfA survey and derived bulge and disc morphological parameters from the azimuthally averaged surface brightness profiles. No statistically significant differences between the Seyfert and control samples are found in either morphological parameters or in light asymmetries (bars, rings, isophotal twisting, etc.), or even in the companion-galaxy properties (magnitude, separation from the host, position angle relative to the host, magnitude difference between the companion and the host, strength of the tidal parameter). They conclude that the nearby environment of Seyfert galaxies is not significantly different from non-active galaxies with the same morphological distribution.

Boris et al. (2002) performed *BVI* surface photometry on a sample of 10 Seyfert 1 galaxies along with narrow-band Hα images of a subsample of six objects. They found that morphologies are confined to early-type galaxies; half of them can be considered as compact; bars are found in only two cases; and average $B - V$ colours are found bluer than those expected for this morphological type (perhaps due to the contribution of the active nucleus and/or the disc to the total luminosity). Evidence of tidal interactions is found in six objects of the sample. They obtain morphological parameters for the nucleus (Gaussian), bulge and disc components finding that in most cases (six out of eight), the disc is best described by a truncated exponential profile. The cut-off is generally associated with the existence of reddened regions (probably dust in the inner few kiloparsecs of the galaxy). Only one galaxy shows disc emission in Hα.

This paper presents a new optical study of the structural parameters of galaxies hosting nuclear emission-line regions. In order to overcome the usual weakness of this kind of study (relatively small and frequently biased samples, uncertainties in the nuclear classification, especially in the control samples), whenever possible, we have tried to supplement our original sample with data from the literature, in particular morphological parameters, and to use a homogeneous, reliable nuclear classification from optical spectroscopy. When data from the literature is used, it is clearly indicated throughout. The paper is structured as follows: first, a description of the original sample and the adopted nuclear classification is outlined; second, a description of the bulge and disc decomposition procedure is given, followed by the results obtained; the discussion section then proceeds, including a thorough analysis of the structural parameters of galaxies hosting nuclear emission-line regions. Our analysis is closed with a discussion on the radial colour distribution of our sample objects. Finally, our conclusions are outlined in Section 6.

2 THE SAMPLE

Our sample (described in Sánchez-Portal et al. 2000 hereafter Paper I) comprises 27 nearby galaxies in a wide range of Hubble

[1] Nevertheless, there is a difference in the slope of the Kormendy relation of active and non-active galaxies at the $\sim 2\,\sigma$ level that is not considered as relevant.

[2] From the control sample, at least two galaxies have been found to be active and at least five objects are nuclear starbursts according to Ho, Filippenko & Sargent (1997).

Table 1. Original and revised nuclear types. S = Seyfert, L = LINER, T = transition nucleus, SB = H II nucleus.

Galaxy	Old type	New type
NGC 3227	S1.5	S1.5
NGC 3516	S1.5	S1.2
NGC 3998	S1.5	L1.9
NGC 7469	S1	S1[a]
NGC 4151	S1.5	S1.5
NGC 5077	S1	L1.9
NGC 6814	S1	S1[a]
NGC 513	S2	S2[a]
NGC 1068	S2	S1.8
Mrk 620 (NGC 2273)	S2	S2
Mrk 622	S2	S2[a]
NGC 3982	S2	S1.9
NGC 5347	S2	S2[a]
NGC 6217	S2	SB
NGC 7479	S2	S1.9
NGC 1052	L	L1.9
NGC 2841	L	L2
M 106 (NGC 4258)	L	S1.9
M 51 (NGC 5194)	L	S2
NGC 7177	L	T2
NGC 7217	L	L2
NGC 2146	SB	SB
NGC 3310	SB	SB
NGC 3353	SB	SB[a]
NGC 1023	Normal	Normal
NGC 6340	Normal	L2
NGC 6384	Normal	T2

[a]Not present in the HFS catalogue

types (from $T = -5$ to $T = 10$) and different level of nuclear activity.

The availability of an accurate and homogeneous nuclear classification is of critical importance when trying to determine the variation of the behaviour of a given physical property across a sample of galaxies with different degrees of activity. To this end, in this paper we have modified the original nuclear classification from Paper I and adopted the nuclear types from Ho et al. (1997) (hereafter HFS), since it provides a reliable homogeneous framework. In addition to H II nuclei, Seyferts and low-ionization nuclear emission regions (LINERs), HFS recognizes a group of 'transition objects', whose [O I] strengths are intermediate between those of H II nuclei and LINERs; transition objects can be most naturally explained as 'normal' LINERs whose integrated spectra are diluted or contaminated by neighbouring H II regions. The HFS survey demonstrates that broad Hα exists not only in Seyfert 1 nuclei but also in LINERs and perhaps even in some transition objects. Accordingly, they propose to extend the 'type 1' and 'type 2' designations, along with the intermediate types (1.2, 1.5, 1.8 and 1.9) to LINERs and transition objects. Table 1 shows the old and current nuclear types. According to the adopted HFS classification, several nuclear types are different from the original ones presented in Paper I. Some objects experience a major modification: NGC 3998 and NGC 5077, formerly considered Seyfert galaxies, become LINERs, while M 106 and M 51, previously classified as LINERs, are now included in the Seyfert category. NGC 6340 and NGC 6384, initially considered normal galaxies, now fall in the LINER class. Nevertheless, the main results outlined in Paper I are not affected.

3 BULGE-TO-DISC DECOMPOSITION PROCEDURE

A spiral or lenticular galaxy can be decomposed to a first approximation into a bulge and a disc. Despite several differences (e.g. greater rotational speed), bulges are generally considered as equivalent to elliptical galaxies due to their morphological similarity, surface brightness distribution and stellar content (Kormendy 1983). Therefore, the same analytical functions are used for ellipticals and bulges of spiral and S0 galaxies. Perhaps the most widely used fitting function is that from de Vaucouleurs (1948):

$$I(r) = I_{\rm e} 10^{-3.33[(r/r_{\rm e})^{1/4}-1]} \quad (1)$$

where $I_{\rm e}$ is the intensity at $r_{\rm e}$, the effective radius. The factor 3.33 is chosen so that half of the total light emitted by the model comes from inside $r_{\rm e}$.

On the other hand, the disc component can be represented by an exponential law (Freeman 1970):

$$I(r) = I_0 {\rm e}^{(-r/r_0)} \quad (2)$$

where I_0 is the disc central surface brightness and r_0 the disc scalelength. Though the reason for an exponential surface brightness distribution is uncertain, it can be derived from a possible solution of the gravitational collapse of a uniform density rotating sphere (see for example, Freeman 1970; Kormendy 1982). Freeman (1970) distinguishes two types of galactic discs: *type I* discs reach $r = 0$ while *type II* do not, showing an inner cut-off. This can be due to an actual lack of mass with low angular momentum, perhaps in the protogalactic cloud, thus leaving a galactic disc with an inner 'hole'. Alternatively, type II discs can be the result of the combination of a pure exponential disc plus an additional component like a lens (Freeman 1976). Kormendy (1977) proposed a formula to fit this kind of disc with internal cut-off, modifying the Freeman expression (equation 2)

$$I(r) = I_0 {\rm e}^{-[r/r_0+(r_{\rm cut}/r)^{\beta}]} \quad (3)$$

where usually $\beta = 3$.

Andredakis, Peletier & Balcells (1995) have fitted the bulge profile with the generalized exponential profile of Sérsic (1968):

$$I(r) = I_0 {\rm e}^{-(r/r_0)^{1/n}} \quad (4)$$

finding that the exponent n varies with the Hubble type; while for early-type spirals, $n = 4$ (standard de Vaucouleurs profile), late-type galaxies show exponential bulges (i.e. $n = 1$). Carollo, Stiavelli & Mack (1998) performed the analysis of the *Hubble Space Telescope* (*HST*) WFPC2 F606W images of a sample of 75 spiral galaxies, ranging from Sa to Sbc. Only a fraction ($\simeq$40 per cent) of the objects contains a smooth, classical $R^{1/4}$ bulge. The central structure of some sample objects presents an irregular morphology: it is often dwarf-irregular-like; in a few cases it is elongated, similar to a late-type bar. In several objects, the spiral structure reaches down to the innermost accessible scales. Occasionally, a small 'bulge-like' feature coexists with the nuclear spiral structure. They found that, in several cases, these inner, morphologically distinct structures are well-fitted by an exponential profile. These exponential bulges embedded in the spiral structure appear to be fainter than $R^{1/4}$ bulges for a given total galactic luminosity and Hubble type.

Two basic methods have been customarily used for obtaining the bulge and disc components from the azimuthally averaged surface brightness profiles: non-linear least-squares fitting and iterative

fitting. In the former method, a non-linear least-squares algorithm is used in order to fit simultaneously both components, while in the latter, an iterative method is applied in order to fit both components independently: a linear least-squares fit is applied first to the region dominated by one of the components; this first model is extrapolated to the whole range, and subtracted from the observed profile, giving a first estimate of the other component, and then the appropriate fitting law is applied, subtracting the obtained model from the observed profile. This residual is then fitted again and the procedure is repeated iteratively until convergence is achieved. The regions where each component dominates over the other should be estimated by visual inspection. Schombert & Bothum (1987) propose a combination of both procedures: first, an iterative procedure is used until convergence is achieved. The resulting bulge and disc parameters are then used as initial estimates for a non-linear least-squares fitting procedure. de Jong (1996) has applied a two-dimensional method using two or three 2D components to model the bulge, disc and (whenever appropriate) bar and applying a non-linear algorithm capable of accepting different weights for each data point. An exponential bulge is proposed instead of the classical $R^{1/4}$ model.

In spite of the disadvantage of the subjective step of visual determination of the ranges of dominance of disc or bulge, we have chosen the iterative fitting procedure because it allows us to control the evolution of the procedure and to exclude regions from the fitting if desired (e.g. regions dominated by a ring or lens, where the profile is not properly described by the sum of a bulge plus a disc). On the other hand, it is possible to detect a disc cut-off (i.e. type II discs). We have used, as an independent variable of the surface brightness profiles, the equivalent radius, defined as $r_{\rm eq} = \sqrt{A/\pi}$, where A is the area enclosed by a given isophote. The most accurate fittings are obtained when there exists a clear range of dominance of one component over the other, i.e. when bulge and disc scalelengths are rather different. In those cases, the fitting has always been started by determining the disc dominance region. On the other hand, for those galaxies where a disc component never dominates, the fitting has been started by a bulge component. In these latter cases, the fitting confidence depends on the accuracy of the $R^{1/4}$ law defining the bulge (Kent 1985). We have also computed the integrated bulge-to-disc luminosity ratio:

$$B/D \equiv \frac{\int_0^\infty I_{\rm bulge}(r) 2\pi r \, {\rm d}r}{\int_0^\infty I_{\rm disc}(r) 2\pi r \, {\rm d}r} = 3.61 \left(\frac{r_{\rm e}}{r_0}\right)^2 \frac{I_{\rm e}}{I_0} \quad (5)$$

where $I_{\rm bulge}(r)$ and $I_{\rm disc}(r)$ are the surface brightness distributions for bulge and disc given by equations (1) and (2). If the galaxy has a type II disc, equation (5) is no longer valid. Instead of using a fitting formula like equation (3) for this kind of disc, we have simply assumed that the galaxy has a sharp cut-off for a certain radius $r = r_{\rm cut}$. Therefore, we change the lower limit of the disc luminosity integral in equation (5), obtaining the expression:

$$B/D = 3.61 \left(\frac{r_{\rm e}}{r_0}\right)^2 \frac{I_{\rm e}}{I_0} \frac{{\rm e}^{r_{\rm cut}/r_0}}{\left(\frac{r_{\rm cut}}{r_0} + 1\right)}. \quad (6)$$

Our computation method assumes that, beyond certain distance from the galaxy centre, the effect of seeing on the surface brightness profile is negligible, and therefore the derived bulge and disc parameters are seeing-free. This assumption is supported by the calculations performed by Capaccioli & de Vaucouleurs (1983); they plotted the convolution function of the light distribution of an idealized E0 galaxy obeying the $R^{1/4}$ law with a single Gaussian seeing point spread function (PSF), for different values of $r_{\rm e}$ and $\sigma_{\rm PSF}$, and showed that there is a radius $r_{\rm ini}(r_{\rm e}, \sigma_{\rm PSF})$ where the difference between the $R^{1/4}$ model and its convolved image becomes negligible. We have estimated $r_{\rm ini}$ using these curves and an initial guess of $r_{\rm e}$ and $\sigma_{\rm PSF}$. Furthermore, we have tried to ensure that our computation is not contaminated by nuclear emission by checking the radial extension of the nuclear Hα emitting regions from our narrow-band surface photometry (see Paper I) and using as initial radius for profile fitting the maximum between $r_{\rm ini}$ and the radial emission extension.

4 RESULTS

Table 2 presents the resulting morphological parameters for the sample galaxies. Magnitudes have been corrected for inclination using the values from Paper I.[3] The computation of profile data-point errors is detailed in Paper I. Parameter errors presented here are those arising from the linear fitting procedure. Fig. 1 shows the results of the bulge–disc decomposition in the I band. The whole set of surface brightness profiles is presented in Paper I.

4.1 Notes on individual objects

4.1.1 Seyfert 1.x galaxies

(i) NGC 3516: we have fitted to this SB0^0 galaxy a Freeman type II disc[4] with $r_{\rm cut} = 5.7$ kpc (25 arcsec).

(ii) NGC 7469: a large excess for $2 \lesssim r \lesssim 6$ kpc is observed in all the surface brightness profiles. Márquez & Moles (1994) attribute this feature to a lens structure, although they did not perform an accurate numerical fitting.

(iii) NGC 4151: as already commented in Paper I, this spiral SABab presents a large-scale bar that affects the surface brightness profile from $r \sim 2.5$ kpc outwards. Therefore, the disc profile is somewhat uncertain.

(iv) NGC 6814: this SABbc galaxy presents a quite compact bulge. This fact, along with the relatively poor seeing (∼2.3 arcsec full width at half maximum (FWHM)) prevented us from obtaining V-band morphological parameters. Márquez et al. (1999) observed this galaxy in the J- and K'-bands, finding bar parameters (PA, ϵ) very similar to ours (see Paper I). Nevertheless, the bulge and disc morphological parameters derived in the NIR are quite different from our optical parameters (though comparable): the bulge and disc equivalent radii lie between 9.2 arcsec and 62 arcsec in the J-band and 5.5 arcsec and 40 arcsec in the K'-band, while our I-band bulge and disc equivalent radius are equal to 2.9 arcsec and 33.8 arcsec, respectively.

(v) NGC 1068: an abrupt fall in the surface brightness profile (see Paper I) is observed at $r \approx 2.2$ kpc, leading to an 'inner' and an 'outer' disc. Alternatively, this feature in the surface brightness profile can be attributed to the existence of a circumnuclear star-forming ring whose intensity peaks around 1.5 kpc (Díaz et al. 2000). This fact, along with the poor seeing conditions during the observations (∼2.2 arcsec FWHM), prevented us from performing an acceptable parameter decomposition.

(vi) NGC 3982: this is the latest type (SABb) galaxy that presents a type II disc. We have applied a fit with $r_{\rm cut} = 12$ arcsec.

[3] $H_0 = 55$ km s^{-1} Mpc^{-1} is used throughout the paper.

[4] As explained before, in all calculations throughout this paper, we have assumed a simplified type II disc with a sharp cut-off at $r_{\rm cut}$.

Table 2. Morphological parameters of the sample galaxies.

Galaxy	Filter	r_e (arcsec) (kpc)	μ_e (mag/arcsec^2)	r_0 (arcsec) (kpc)	μ_0 (mag/arcsec^2)	*B/D*
NGC 3227	V	1.614 ± 0.136 0.165 ± 0.014	18.267 ± 0.223	23.317 ± 0.630 2.378 ± 0.064	20.56 ± 0.047	0.143
	R	1.745 ± 0.144 0.178 ± 0.015	17.783 ± 0.217	23.313 ± 0.671 2.378 ± 0.068	20.107 ± 0.047	0.172
	I	2.601 ± 0.070 0.265 ± 0.007	18.144 ± 0.069	23.404 ± 0.511 2.387 ± 0.052	19.546 ± 0.045	0.162
NGC 3516	V	8.948 ± 0.295 2.070 ± 0.068	20.041 ± 0.066	21.447 ± 0.439 4.962 ± 0.102	21.940 ± 0.036	5.354
	R	7.472 ± 0.217 1.729 ± 0.050	19.269 ± 0.062	24.836 ± 1.385 5.747 ± 0.081	21.875 ± 0.074	4.911
	I	8.491 ± 0.179 1.965 ± 0.041	18.892 ± 0.043	18.314 ± 2.217 4.238 ± 0.513	20.906 ± 0.219	8.212
NGC 3982	V	27.202 ± 1.417 2.662 ± 0.139	22.512 ± 0.065	8.303 ± 0.266 0.812 ± 0.026	18.631 ± 0.106	1.884
	R	21.741 ± 0.962 2.127 ± 0.094	21.748 ± 0.058	8.288 ± 0.198 0.810 ± 0.019	18.221 ± 0.077	1.677
	I	19.239 ± 0.189 1.882 ± 0.018	20.963 ± 0.013	8.481 ± 0.241 0.830 ± 0.023	17.874 ± 0.087	1.841
NGC 7469	V	2.062 ± 0.057 0.882 ± 0.024	18.097 ± 0.065	30.772 ± 3.025 13.161 ± 1.294	21.508 ± 0.102	0.375
	R	1.635 ± 0.029 0.699 ± 0.012	16.904 ± 0.044	33.873 ± 7.090 14.487 ± 3.032	21.652 ± 0.178	0.667
	I	1.609 ± 0.057 0.688 ± 0.024	16.332 ± 0.088	15.399 ± 2.102 6.586 ± 0.899	20.222 ± 0.239	1.419
NGC 4151	V	10.320 ± 0.987 0.907 ± 0.087	20.001 ± 0.155	39.771 ± 2.080 3.495 ± 0.183	20.985 ± 0.035	0.602
	R	6.100 ± 0.346 0.536 ± 0.030	18.703 ± 0.102	27.596 ± 1.176 2.425 ± 0.103	20.189 ± 0.043	0.693
	I	9.852 ± 0.222 0.866 ± 0.019	18.921 ± 0.035	40.326 ± 2.155 3.544 ± 0.189	19.947 ± 0.037	0.554
M 106 (NGC 4258)	V	12.732 ± 0.627 0.503 ± 0.025	20.235 ± 0.079	62.609 ± 9.662 2.472 ± 0.381	20.163 ± 0.114	0.140
	R	13.777 ± 0.609 0.544 ± 0.024	19.966 ± 0.070	63.880 ± 7.346 2.523 ± 0.290	19.783 ± 0.083	0.142
	I	14.787 ± 0.426 0.584 ± 0.017	19.403 ± 0.044	57.365 ± 4.728 2.265 ± 0.187	18.994 ± 0.067	0.165
NGC 6814	V	–	–	–	–	–
	R	2.386 ± 0.196 0.329 ± 0.027	17.862 ± 0.204	20.509 ± 1.732 2.826 ± 0.239	18.955 ± 0.159	0.134
	I	2.908 ± 0.353 0.401 ± 0.049	17.523 ± 0.296	20.116 ± 0.104 2.771 ± 0.014	18.320 ± 0.010	0.157
Mrk 620 (NGC 2273)	V	1.990 ± 0.696 0.322 ± 0.112	18.825 ± 0.918	11.676 ± 0.336 1.893 ± 0.054	19.475 ± 0.062	0.191
	R	1.702 ± 0.165 0.276 ± 0.027	17.829 ± 0.265	11.820 ± 0.458 1.916 ± 0.074	19.102 ± 0.088	0.242
	I	1.677 ± 0.100 0.272 ± 0.016	16.942 ± 0.156	11.787 ± 0.371 1.911 ± 0.060	18.488 ± 0.069	0.304
Mrk 622	V	4.486 ± 0.113 2.754 ± 0.070	20.807 ± 0.049	1.882 ± 0.105 1.155 ± 0.064	16.110 ± 0.496	13.694
	R	3.787 ± 0.075 2.324 ± 0.046	20.033 ± 0.040	2.340 ± 0.189 1.436 ± 0.116	17.344 ± 0.584	15.330
	I	3.730 ± 0.085 2.290 ± 0.052	19.496 ± 0.047	4.653 ± 0.871 2.856 ± 0.535	19.869 ± 0.670	10.350
M 51 (NGC 5194)	V	8.989 ± 0.805 0.36 ± 0.033	20.434 ± 0.151	17.811 ± 0.792 0.727 ± 0.032	17.992 ± 0.066	–
	R	7.371 ± 0.510 0.301 ± 0.021	19.786 ± 0.108	14.475 ± 0.582 0.591 ± 0.024	17.337 ± 0.056	–
	I	6.829 ± 0.600 0.279 ± 0.024	19.031 ± 0.153	14.421 ± 0.474 0.588 ± 0.019	16.714 ± 0.050	–

Table 2 – *continued*

Galaxy	Filter	r_e (arcsec) (kpc)	μ_e (mag/arcsec^2)	r_0 (arcsec) (kpc)	μ_0 (mag/arcsec^2)	*B/D*
NGC 1052	V	38.554 ± 0.964 4.996 ± 0.125	21.918 ± 0.036	–	–	–
	R	35.321 ± 0.955 4.577 ± 0.124	21.287 ± 0.040	–	–	–
	I	28.426 ± 1.042 3.683 ± 0.135	20.285 ± 0.055	–	–	–
NGC 2841	V	33.019 ± 0.735 1.857 ± 0.041	21.513 ± 0.030	54.806 ± 12.437 3.082 ± 0.699	21.344 ± 0.151	1.121
	R	29.150 ± 0.456 1.639 ± 0.026	20.870 ± 0.022	49.690 ± 7.206 2.794 ± 0.405	20.726 ± 0.110	1.088
	I	26.658 ± 0.371 1.499 ± 0.021	20.052 ± 0.020	54.313 ± 2.231 3.054 ± 0.125	19.952 ± 0.026	0.793
NGC 3998	V	10.363 ± 0.267 0.973 ± 0.025	19.365 ± 0.048	17.987 ± 1.064 1.689 ± 0.100	20.173 ± 0.139	5.011
	R	9.627 ± 0.188 0.904 ± 0.018	18.797 ± 0.036	17.120 ± 1.099 1.607 ± 0.103	19.746 ± 0.157	5.734
	I	9.855 ± 0.178 0.925 ± 0.017	18.098 ± 0.033	17.404 ± 1.355 1.634 ± 0.127	19.079 ± 0.187	5.880
NGC 5077	V	16.889 ± 0.598 4.216 ± 0.149	21.201 ± 0.059	–	–	–
	R	15.385 ± 0.362 3.841 ± 0.090	20.468 ± 0.040	–	–	–
	I	15.355 ± 0.466 3.883 ± 0.116	20.095 ± 0.051	–	–	–
NGC 6340	V	9.251 ± 0.326 0.976 ± 0.034	20.486 ± 0.066	22.669 ± 0.325 2.392 ± 0.034	20.150 ± 0.029	0.441
	R	8.488 ± 0.238 0.896 ± 0.025	19.926 ± 0.054	22.088 ± 0.269 2.331 ± 0.028	19.756 ± 0.026	0.455
	I	8.610 ± 0.190 0.908 ± 0.020	19.227 ± 0.041	23.031 ± 0.340 2.430 ± 0.036	19.090 ± 0.030	0.445
NGC 6384	V	9.788 ± 0.352 1.435 ± 0.052	20.535 ± 0.072	27.015 ± 1.979 3.960 ± 0.290	20.619 ± 0.108	0.512
	R	2.981 ± 0.337 0.437 ± 0.049	17.768 ± 0.307	2.931 ± 1.645 3.361 ± 0.241	19.671 ± 0.143	0.352
	I	4.957 ± 0.245 0.727 ± 0.036	18.252 ± 0.118	21.506 ± 1.229 3.153 ± 0.180	19.138 ± 0.106	0.434
NGC 7177	V	12.885 ± 1.254 1.305 ± 0.127	20.913 ± 0.170	10.897 ± 0.210 1.104 ± 0.021	19.777 ± 0.057	1.772
	R	11.598 ± 1.018 1.175 ± 0.103	20.253 ± 0.158	11.588 ± 0.318 1.175 ± 0.032	19.580 ± 0.074	1.946
	I	6.547 ± 0.479 0.663 ± 0.049	18.575 ± 0.153	11.169 ± 0.325 1.131 ± 0.033	18.541 ± 0.083	1.202
NGC 7217	V	20.358 ± 1.611 1.697 ± 0.134	20.885 ± 0.121	19.623 ± 0.570 1.636 ± 0.047	19.220 ± 0.059	0.838
	R	30.241 ± 2.622 2.521 ± 0.219	20.878 ± 0.120	19.863 ± 0.648 1.656 ± 0.054	19.029 ± 0.065	1.525
	I	38.220 ± 2.514 3.187 ± 0.210	20.487 ± 0.086	17.819 ± 0.636 1.486 ± 0.053	18.481 ± 0.079	2.617
NGC 2146	V	–	–	–	–	–
	R	–	–	–	–	–
	I	8.444 ± 1.322 0.665 ± 0.104	20.351 ± 0.278	20.136 ± 1.055 1.585 ± 0.083	19.173 ± 0.092	0.214
NGC 3310	V	1.950 ± 0.049 0.168 ± 0.004	18.431 ± 0.045	12.808 ± 0.637 1.106 ± 0.055	19.382 ± 0.185	0.201
	R	2.042 ± 0.211 0.176 ± 0.018	18.058 ± 0.187	13.346 ± 0.975 1.153 ± 0.084	19.245 ± 0.231	0.252
	I	2.563 ± 0.305 0.221 ± 0.026	17.932 ± 0.205	12.357 ± 0.567 1.067 ± 0.049	18.679 ± 0.175	0.309

Table 2 – *continued*

Galaxy	Filter	r_e (arcsec) (kpc)	μ_e (mag/arcsec^2)	r_0 (arcsec) (kpc)	μ_0 (mag/arcsec^2)	*B/D*
NGC 6217	V	0.708 ± 0.019	16.528 ± 0.084	21.276 ± 1.176	20.137 ± 0.058	0.111
		0.085 ± 0.002		2.554 ± 0.141		
	R	1.425 ± 0.057	17.818 ± 0.105	20.557 ± 1.035	19.805 ± 0.054	0.108
		0.171 ± 0.007		2.468 ± 0.124		
	I	3.192 ± 0.109	18.974 ± 0.075	20.353 ± 0.770	19.276 ± 0.041	0.117
		0.383 ± 0.013		2.443 ± 0.092		
NGC 1023	V	21.680 ± 0.872	20.627 ± 0.058	29.703 ± 1.879	20.506 ± 0.062	1.721
		1.217 ± 0.049		1.667 ± 0.105		
	R	19.607 ± 0.673	19.967 ± 0.051	27.754 ± 1.662	19.979 ± 0.064	1.822
		1.101 ± 0.038		1.558 ± 0.093		
	I	19.731 ± 0.253	19.333 ± 0.019	25.952 ± 0.903	19.354 ± 0.040	2.127
		1.108 ± 0.014		1.457 ± 0.051		

4.1.2 Seyfert 2 galaxies

(i) NGC 513: in Paper I we classified this galaxy as SABa. We failed to perform a simple bulge+disc decomposition, but perhaps this galaxy has a type II disc or additional components like a ring or lens.

(ii) Mrk 622: according to Paper I, we classified this galaxy as SB0. We have fitted a type II disc with $r_{cut} = 11$ arcsec.

(iii) M 51: the overall disc does not obey an exponential law. For $r > 40$ arcsec the galaxy shows a flat profile, while for smaller radii the surface brightness distribution can be fitted to an exponential profile with small scalelength. This behaviour has also been reported by Boroson (1981), who finds a flat disc for $r > 52$ arcsec. The shape of the surface brightness profile can be explained by the presence of a nearby companion galaxy, NGC 5195.

(iv) NGC 5347: the outstanding bar present in this SBab galaxy made it impossible to perform a bulge+disc parameter decomposition. The K' image from Márquez et al. (1999) only shows a large bar also observed in our optical images. Their NIR bar parameters (PA, ϵ) match our optical parameters (Paper I). They are able to derive bulge and disc morphological parameters: the bulge and disc equivalent radius lie between 7.9 arcsec and 23 arcsec, respectively, in the *J*-band and 2.2 arcsec and 19 arcsec in the K'-band.

(v) NGC 7479: as in the previous case, this SBc has a very strong bar that dominates the surface profile. Therefore, it was not possible to perform an acceptable parameter decomposition.

4.1.3 LINERs

(i) NGC 3998: we have fitted to this SA0^0 galaxy a Freeman type II disc with $r_{cut} = 2.75$ kpc (30 arcsec).

(ii) NGC 5077: this E3–4 galaxy is the main member in a group of eight; a luminosity excess (halo) is detected from $r \sim 5$ kpc outwards (Fig. 1).

(iii) NGC 7177: the surface brightness profile lies below the $R^{1/4}$ law for $r < 3.8$ arcsec; this behaviour cannot be explained in terms of a seeing effect: we have computed the expected light distribution for a pure $R^{1/4}$ bulge with $r_e \approx 6.5$ arcsec convolved with the same seeing PSF (about 1.2 arcsec FWHM) finding that the expected profile flattening begins about $r \approx 0.65$ arcsec. Therefore, the observed flattening seems to be an intrinsic bulge characteristic.

5 DISCUSSION

5.1 Bulge and disc parameters of active and normal galaxies

5.1.1 The extended sample

In order to perform a detailed study of the behaviour of bulge and disc parameters across all levels of nuclear activity, we have increased our sample by compiling from the literature a large number of morphological parameters belonging to galaxies contained in the HFS catalogue. Our main source of data is the set of bulge and disc parameters from Baggett, Baggett & Anderson (1998) (hereafter BBA) that comprises 659 galaxies, from which we have selected bulge and disc parameters for the 234 objects contained in the HFS catalogue.

The extended sample contains 261 galaxies hosting all levels of nuclear activity. According to the classification of HFS the sample contains 22 Seyfert 1, 16 Seyfert 2, 90 LINERs, 108 starburst and H II galaxies and 25 normal galaxies. Therefore, there is an excess of low-activity nuclei.

BBA parameters were derived using profiles obtained from major-axis cuts of two-dimensional digital images created from photographic plates (photographic *V*-band) from the PANBG catalogue Kodaira, Okamura & Ichikawa (1990). The field size is large but the spatial resolution is quite poor (1 arcsec per pixel), as is the mean seeing, about 4 arcsec FWHM. On the other hand, our results were obtained from azimuthally averaged profiles of CCD images with good spatial resolution (0.3 arcsec per pixel), much better mean seeing ($\sim$1.45 arcsec FWHM) but reduced field of view, limiting the maximum profile radius to about 80 arcsec. Therefore, we can expect from BBA data a better disc sampling while our profiles would provide more accurate bulge results.

Due to the differences shown above, in some cases large discrepancies between our results and those from BBA appear, as shown in Fig. 2.

The sample morphological distribution is shown in Fig. 3. The results of a χ^2 test on the distribution for the different nuclear types is presented in Table 3. Seyfert 1 and Seyfert 2 galaxies are drawn from the same morphological distribution at the 99 per cent confidence level; Seyfert 2 and LINERs are also drawn from the same distribution at nearly 99 per cent confidence level; Seyfert 1 and LINERs follow the same distribution at a lower confidence level ($\simeq$79 per cent); on the other hand, the remaining nuclear types clearly present

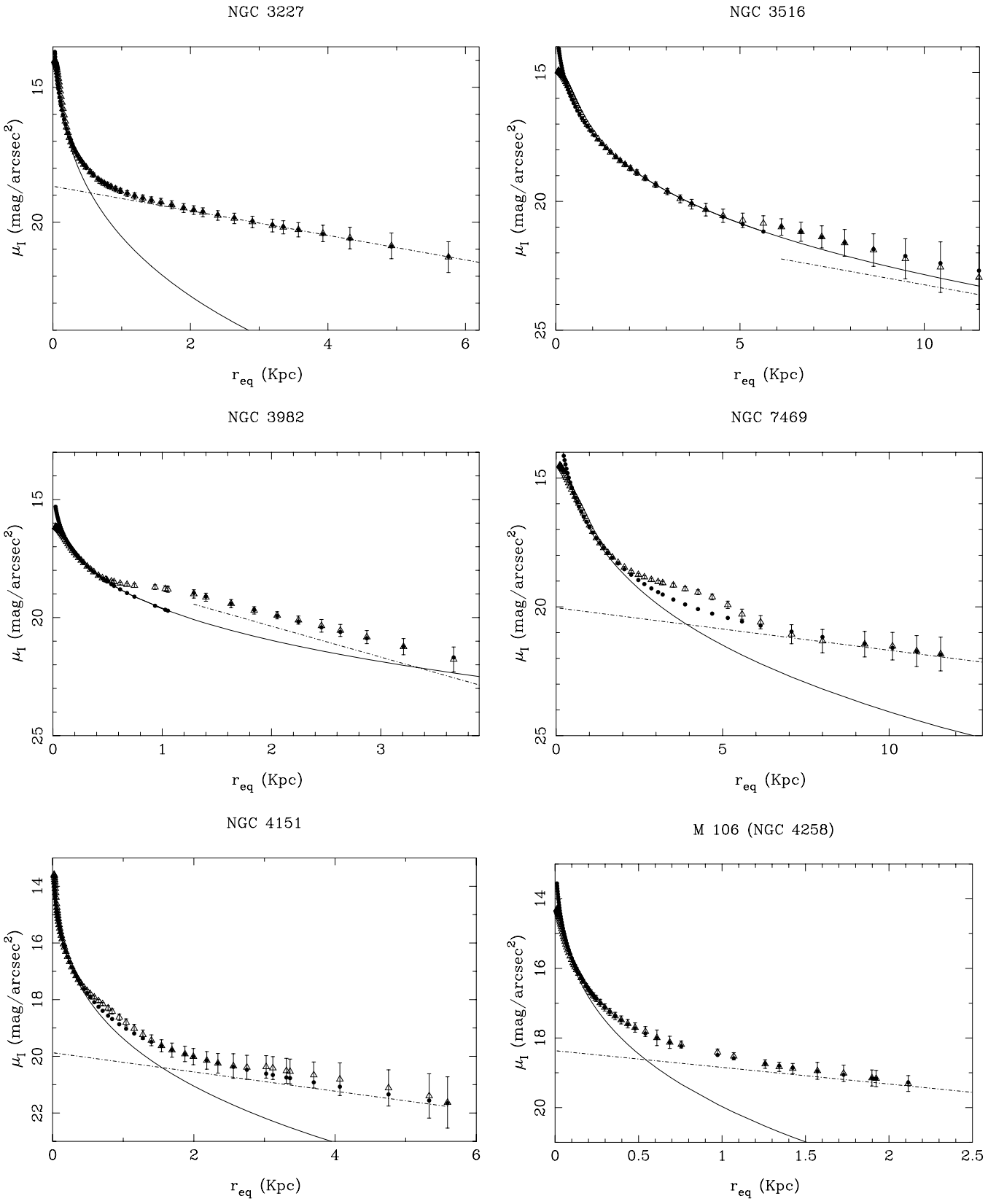

Figure 1. *I*-band parameter decomposition. Triangles represent the calibrated surface brightness profile, the solid line shows the bulge model, the dash-dotted line represents the disc model and filled circles show the sum of bulge and disc models.

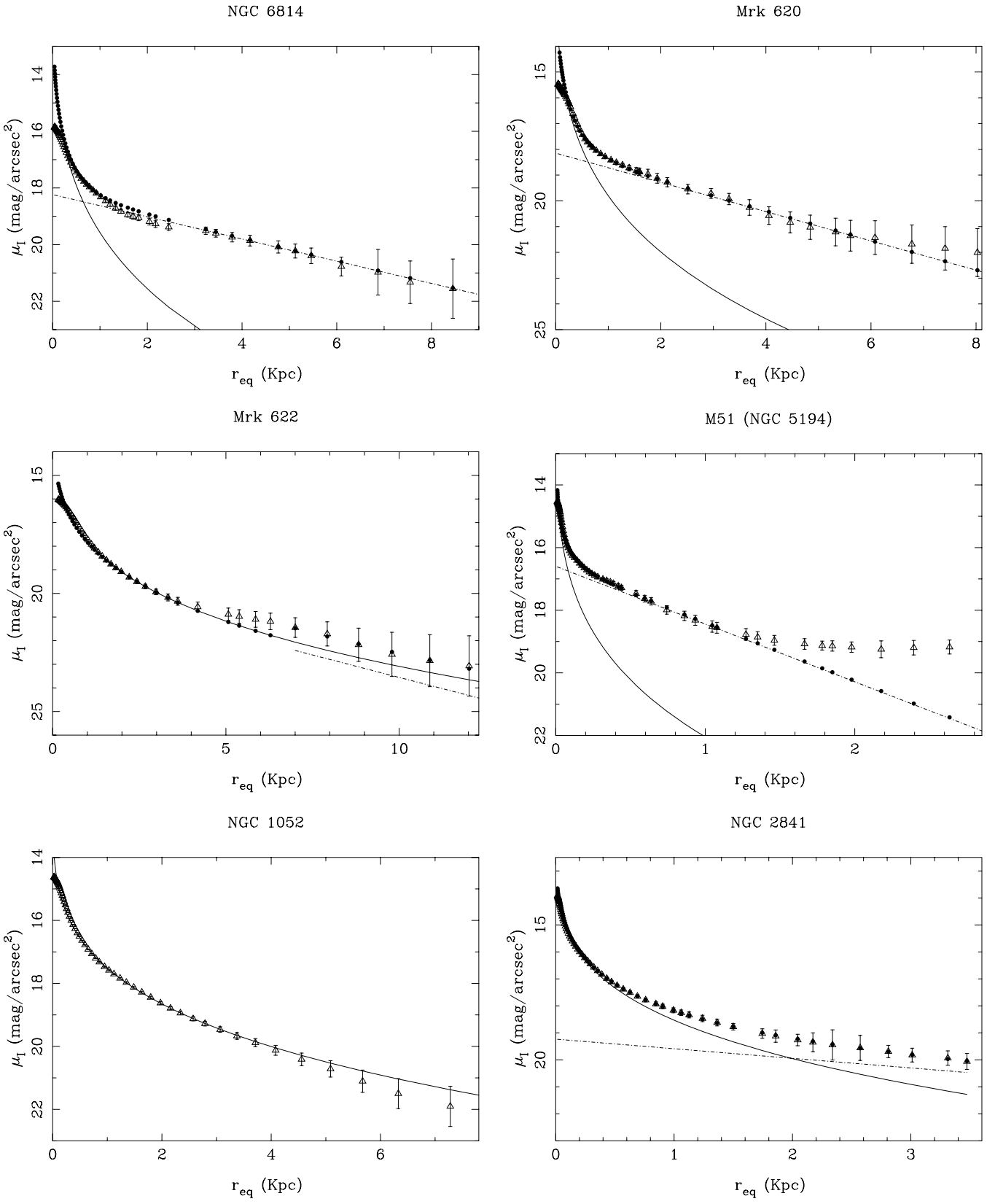

Figure 1 – *continued*

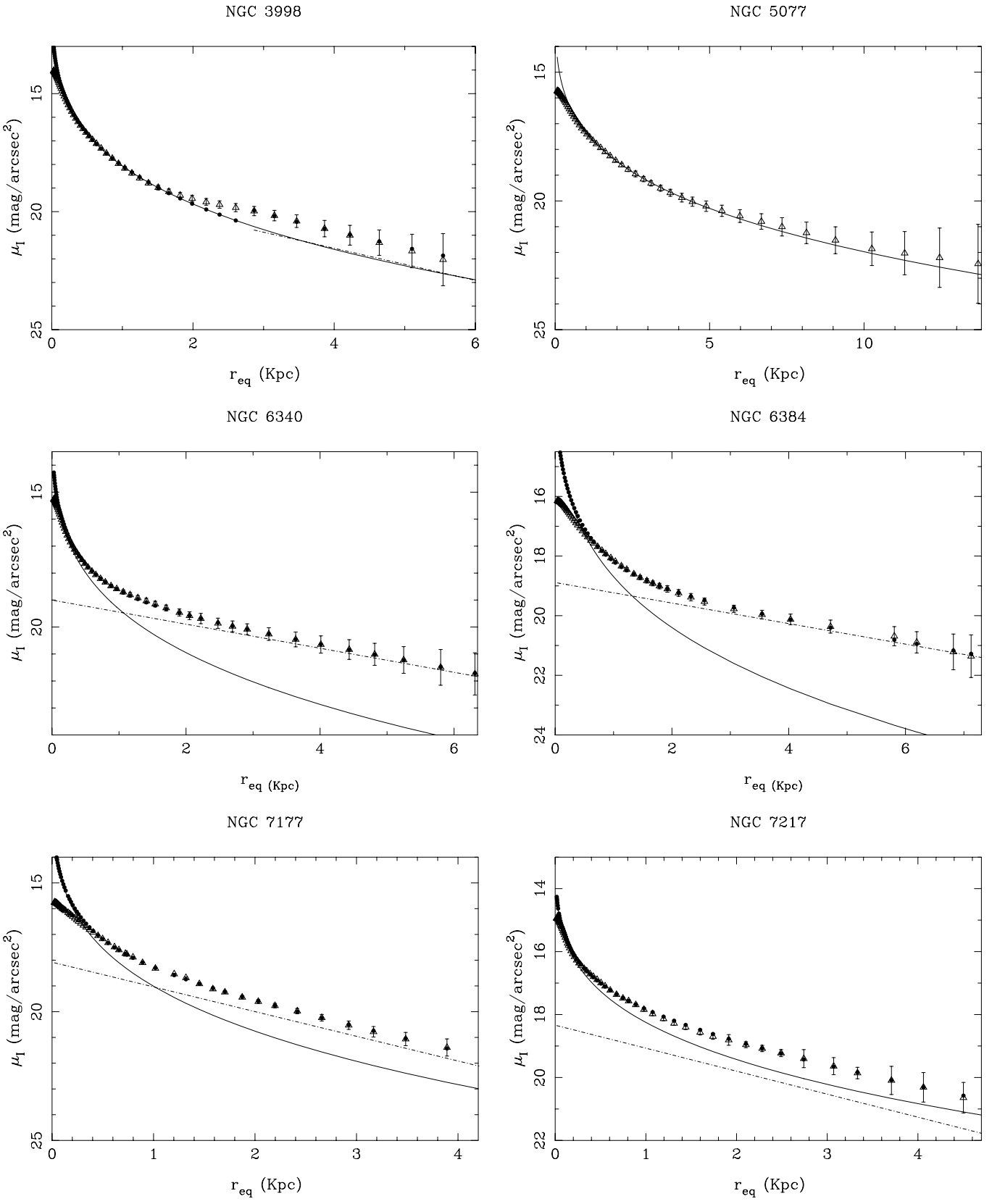

Figure 1 – *continued*

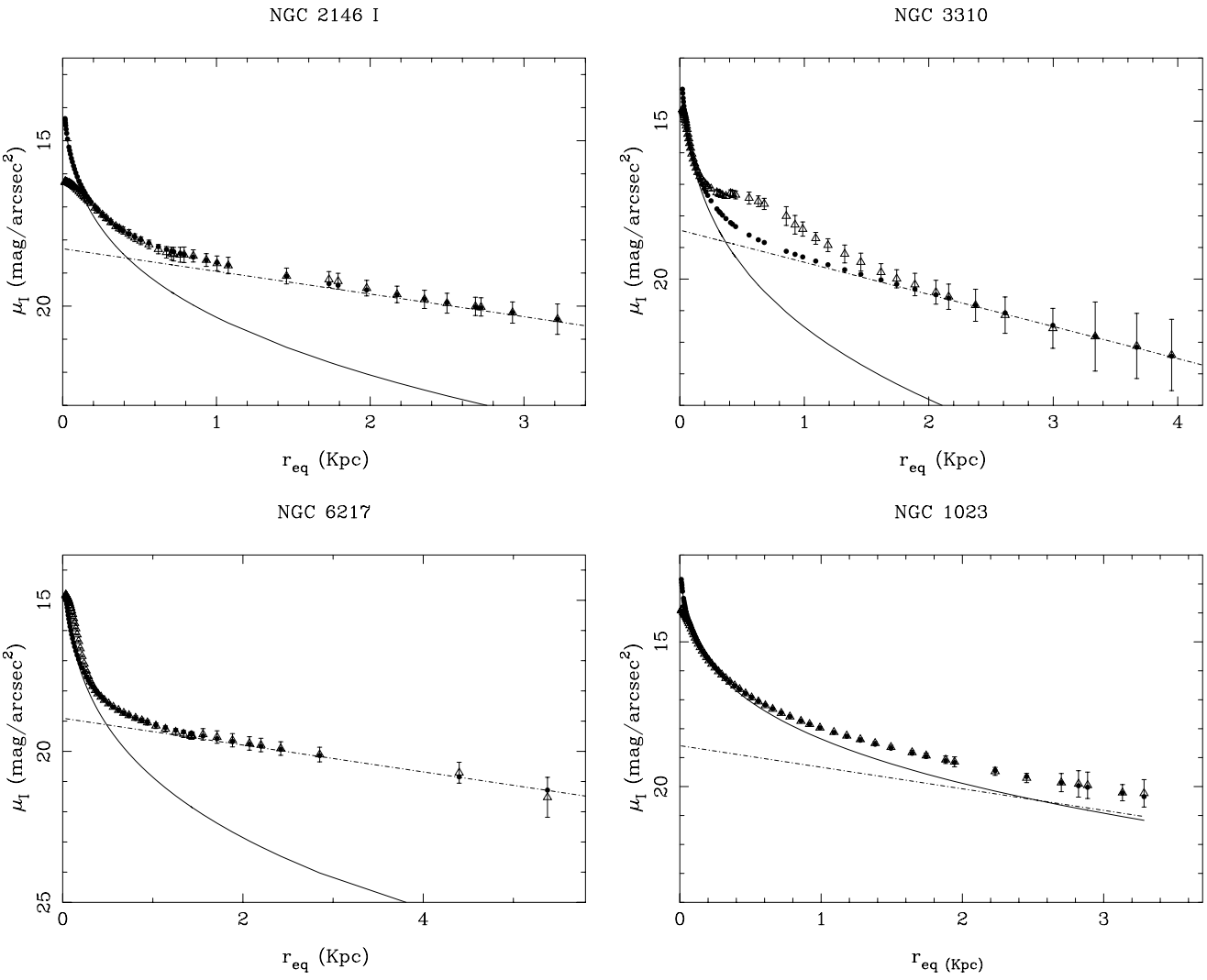

Figure 1 – *continued*

different morphological type distributions. This should be taken into account when analysing the distribution of bulge and disc parameters.

According to HFS, all spiral galaxies show nuclear emission lines. Normal galaxies (with no emission lines in the nuclear spectrum) are only observed in the earliest Hubble types ($T \leqslant 0$). Most AGN reside in early-type galaxies (E-Sbc) while starbursts are generally observed in later-type galaxies.

As an independent comparison sample, we have added the *V* and *I* data from Xanthopoulos (1996) and from Mediavilla et al. (1989). The former sample comprises Seyfert type 1 and 2 galaxies from Véron-Cetty & Véron (2000), with declination between -55° and $+8^\circ$ and redshift $z \leqslant 0.043$. Hubble types range from -2 (S0) to 5 (Sc); the latter also comprises Seyfert 1 and 2 galaxies from Adams (1977), with redshift $z \leqslant 0.08$. This sample includes one E galaxy, one N-type galaxy and several disc galaxies with Hubble type ranging from -2 (S0) to 4 (Sbc). This complementary data set comprises 21 Seyfert 1 and 12 Seyfert 2 galaxies.

5.1.2 Disc and bulge parameters

We have performed a statistical analysis on the individual morphological parameter distributions by means of a series of Kolmogorov–Smirnov tests. The results are shown in Table 4. It should be recalled that the distribution of morphological types across Seyfert 1, Seyfert 2 and LINER galaxies is quite homogeneous, but that is not true when compared with starbursts and normal galaxies (see Table 3). Seyfert 1 and Seyfert 2 effective radii and scalelengths are drawn from the same distribution (null hypothesis) at about the 97 per cent and 91 per cent confidence level, respectively. On the other hand, while bulges of Seyfert 1 galaxies and LINERs follow the same distribution at about the 96 per cent confidence level, disc distributions are most likely different (the null hypothesis is rejected at the 48 per cent confidence level). Seyfert 2 and LINER bulge effective radii are drawn from the same distribution only at less than the 70 per cent level, while disc scalelengths follow the same distribution at about the 90 per cent level. When comparing active (i.e. Seyfert 1, Seyfert 2 and LINER) galaxies with non-active (i.e. starburst and normal) galaxies, the distributions of morphological parameters are generally different (with some exceptions, e.g. disc scalelengths of Seyfert 2 and normal galaxies). As a conclusion, we cannot claim that the individual morphological parameters of active and non-active galaxies follow the same statistical distribution, as other authors do (e.g. Virani et al. 2000).

Perhaps more interesting than the statistics shown above, the distribution of morphological parameters in the (μ_0, log r_0) and

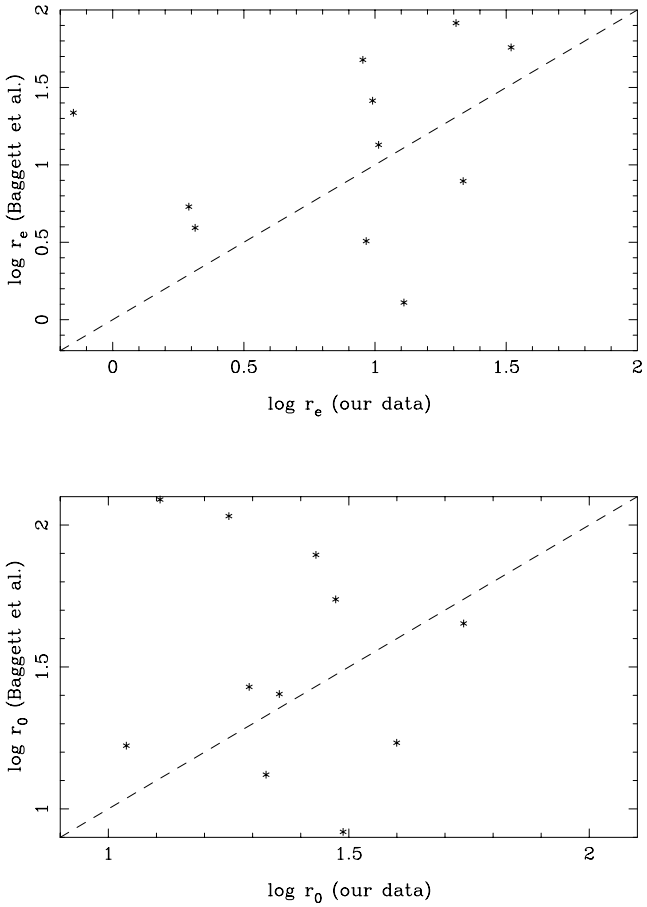

Figure 2. Comparison between disc (r_0) and bulge parameters (r_e) from our data and BBA data.

(μ_e, log r_e) planes can be studied. Disc parameters are strongly clustered (perhaps a selection effect due to the luminosity-limited sample) but there is only a weak linear correlation in the (μ_0, log r_0) plane, as shown in Fig. 4.

On the other hand, bulge parameters show a strong linear correlation that constitutes the projection in the (μ_e, log r_e) parameter subspace of the 'fundamental plane' of ellipticals and bulges of spiral and lenticular galaxies.

We have performed a fit of the relation between bulge parameters μ_e versus log r_e by means of linear regression for the different nuclear types. The results are shown in Fig. 5. We can observe the following.

(i) The spheroidal component of starbursts constitutes a lower luminosity class. It is clear in Fig. 5 that starbursts follow a distribution that lies parallel and below the overall sample. This could be related to the fact that starburst galaxies tend to be late-type galaxies, as seen in Fig. 3.

(ii) LINERs and normal galaxies follow very similar distributions (differences in slope are smaller than 0.2σ and $\sim\sigma$ in zero-point).

(iii) We can observe differences in the slope of the distributions of Seyfert 1, Seyfert 2, LINERs and normal galaxies. When comparing Seyfert 1 with LINERs and normal galaxies, the differences are of order σ and can be due to statistical errors. Differences between the Seyfert 2 distribution and that of LINERs and normal galaxies are more significant, at the $\gtrsim 2.5\ \sigma$ level. On the other hand, there is a difference at the $\sim\sigma$ level in the slope of the distribution of Seyfert 1 and Seyfert 2 that can also be attributed to statistical uncertainties. Nevertheless, equivalent fits performed in both *V* and *I* bands in our comparison sample lead to a very similar result at the $\sim 2\ \sigma$ significance level (see Fig. 6). Therefore, we have observed that the different classes of galaxies (Seyfert 1, Seyfert 2, LINERs and normal galaxies) show different bulge distributions in the (μ_e, log r_e) plane. While sometimes this difference has little statistical significance, in the case of Seyfert 2 galaxies it is more important, since it cannot be solely attributed to statistical effects. If real, the observed distribution difference could imply families of bulges with different physical properties, as proposed for bright and faint cluster ellipticals (Hoessel, Oegerle & Schneider 1987). Capaccioli, Caon & D'Onofrio (1992) also describe two physically different families of ellipticals, early-type dwarfs and bulges of SOs and spirals, each family described by a different relation in the (μ_e, log r_e) plane. One of the families comprises the cluster brightest cD and quasar-hosting galaxies, while the other comprises normal ellipticals, fainter bulges and early-type dwarfs. According to these authors, the latter objects are in the latest stages of dissipative collapse, while the former ones have experienced merging and accretion processes.

The stellar kinematics in the nuclei of Seyfert galaxies both of types 1 and and 2 seems to be similar to that in normal galaxies, with active and non-active galaxies following the same Faber–Jackson relation (Terlevich, Díaz & Terlevich 1990; Nelson & Whittle 1996). Further evidence of the similarity of stellar kinematics in active and normal galaxies has been provided by Ferrarese et al. (2001). They studied the $M_\bullet - \sigma$ relation for AGN, an empirical correlation between the central black hole mass and the stellar velocity dispersion, finding good agreement between black hole masses derived from reverberation mapping and from the $M_\bullet - \sigma$ relation as derived from normal and weakly active galaxies, indicating a common relationship between active and quiescent black holes and their host galaxy environment. Regarding gas motions, the relation between the velocity dispersion of the gas in the NLR and the stellar velocity dispersion and for galaxies of Seyfert types 1 and 2 shows a large scatter although clustered around the 1:1 line (Jiménez-Benito et al. 2000). This suggests that gas motions are mainly controlled by the mass of the galactic bulge along with other agents, like shock waves, that may be produced by the interaction of jets with ambient gas, or tidal interactions with companions, providing an additional line broadening. Yet, the kinematics of the two main types of Seyfert galaxies show some differences that need to be explained: a ratio between gas and stellar velocity dispersions larger than one is common in Seyfert type 2 nuclei, while some Seyfert type 1 nuclei show emission lines which are narrower than the stellar absorption lines.

5.1.3 Type II discs

As shown in Section 4.1 we have found type II discs in three Seyfert galaxies and in one LINER from our original sample. Since no type II disc was detected in non-active (i.e. starburst or normal) galaxies, we have investigated the possible connection between nuclear activity and the existence of type II discs. The BBA sample parameters were derived using the modified Kormendy function (equation 3) and a large fraction of the objects ($\simeq$50 per cent) presents a type II disc.

Tables 5 and 6 show the statistics of type II discs in the extended sample. As shown in Table 5, we do not find a correlation between the existence of type II discs and nuclear activity. In fact, the highest fraction of type II discs is found in normal galaxies. Nevertheless, we do find a greater incidence of type II discs in earlier morphological types ($T = -3$ to $T = 0$) as shown in Table 6.

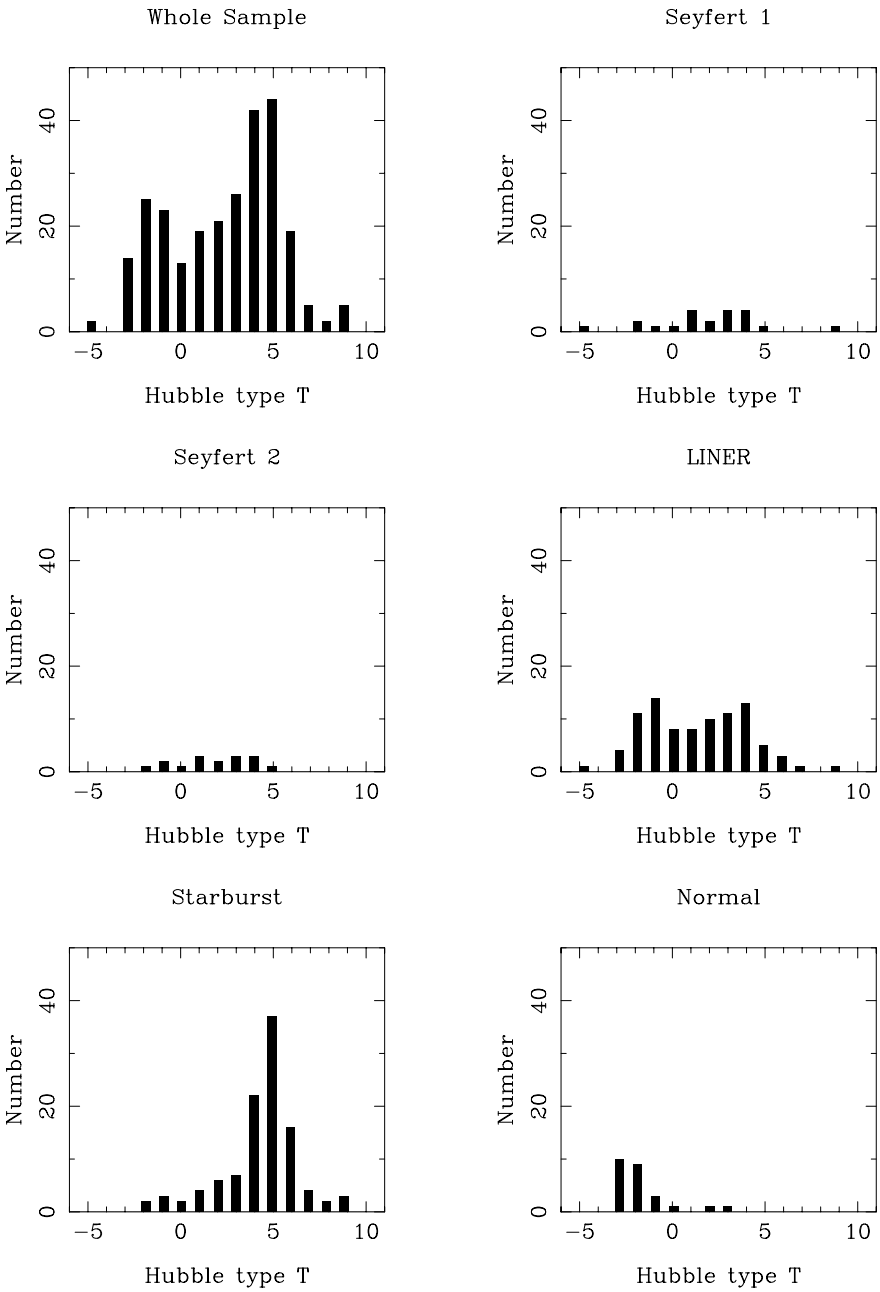

Figure 3. Distribution of morphological Hubble types of the extended sample galaxies.

5.1.4 B/D relation

We have derived the B/D relation by means of equation (6). As comparison values, we have used the mean values obtained by Simien & de Vaucouleurs (1986) (hereafter SDV); these values served as a reference data set, rejecting all morphological parameters leading to B/D values highly deviated from SDV data. Nevertheless, it is worth mentioning that SDV B/D values present a large scatter, mainly attributed to errors in the surface photometry and in the decomposition process and, to a lesser extent, to morphological classification errors.

The distribution of B/D values is shown in Fig. 7 (left panel). As can be observed in Table 4, the B/D relation values for Seyfert 1 and Sefyert 2 galaxies are drawn from the same distribution at

Table 3. Chi-square test on the morphological distribution for the different nuclear types.

Comparison types	χ^2	Significance
S1 versus S2	2.408	0.992
S1 versus LINER	8.643	0.799
S1 versus starburst	29.920	0.005
S1 versus normal	29.182	0.002
S2 versus LINER	4.314	0.987
S2 versus starburst	22.016	0.037
S2 versus normal	24.120	0.004
LINER versus starburst	64.457	0.000
LINER versus normal	38.634	0.000
Starburst versus normal	96.736	0.000

Table 4. Kolmogorov–Smirnov test on the distribution of morphological parameters.

Comparison	μ_e		r_e		μ_0		r_0		B/D	
Types	K–S	Significance	K–S	Significance	K–S	Significance	K–S	Significance	K–S	Significance
S1 versus S2	0.227	0.725	0.148	0.988	0.317	0.440	0.167	0.985	0.245	0.786
S1 versus LINER	0.127	0.941	0.121	0.961	0.188	0.627	0.188	0.627	0.233	0.356
S1 versus starburst	0.202	0.489	0.256	0.216	0.211	0.444	0.345	0.037	0.300	0.122
S1 versus normal	0.280	0.328	0.295	0.269	0.200	0.819	0.250	0.560	0.647	0.001
S2 versus LINER	0.209	0.596	0.196	0.677	0.267	0.448	0.171	0.921	0.297	0.366
S2 versus starburst	0.253	0.366	0.275	0.271	0.311	0.248	0.300	0.287	0.445	0.046
S2 versus normal	0.292	0.388	0.312	0.306	0.433	0.120	0.200	0.925	0.455	0.112
LINER versus starburst	0.219	0.043	0.266	0.007	0.121	0.522	0.185	0.092	0.402	0.000
LINER versus normal	0.303	0.063	0.283	0.099	0.288	0.142	0.162	0.792	0.467	0.003
Starburst versus normal	0.427	0.003	0.250	0.206	0.239	0.293	0.181	0.646	0.847	0.000

86 per cent confidence level. On the other hand, Seyfert and LINER B/D distributions are most likely different since the null hypothesis is rejected at about the 26 per cent and 37 per cent confidence level for Seyfert 1 and Seyfert 2, respectively.

As can be observed in Fig. 7 and in the mean deviation estimators shown in Table 7, B/D values spread over a large range, especially for the earliest morphological types (T < 0). In order to avoid the effects of outliers, we have used the median $(B/D)_{\rm median}$ rather than the mean as a robust average estimator. As shown in Table 7 and in the right panel of Fig. 7, a descending trend is observed in $(B/D)_{\rm median}$ with the Hubble type T, as expected from the definition of the latter as a sequence of decreasing importance of the spheroidal component with respect to the disc. This trend is also reflected in SDV data. Our median values are generally higher than those derived by SDV (see Table 7); this can be at least partially explained by the fact that we allow for the existence of type II discs (not considered by SDV); on the other hand, SDV values are derived from the *B*-band while ours are computed from *V*-band surface profiles. From Table 7 and Fig. 7 we can observe that:

(i) The distribution of $(B/D)_{\rm median}$ seems to be generally independent of the nuclear type.

(ii) Nevertheless, for the earliest morphological types ($T < 0$), Seyfert galaxies tend to have a higher $(B/D)_{\rm median}$ relation (greater relative importance of the spheroidal component) than the remaining types.

(iii) Starburst galaxies show smaller $(B/D)_{\rm median}$ values than the remaining nuclear species for the earliest Hubble types ($T < 0$) and approximately constant between $T = -1$ and $T = 3$.

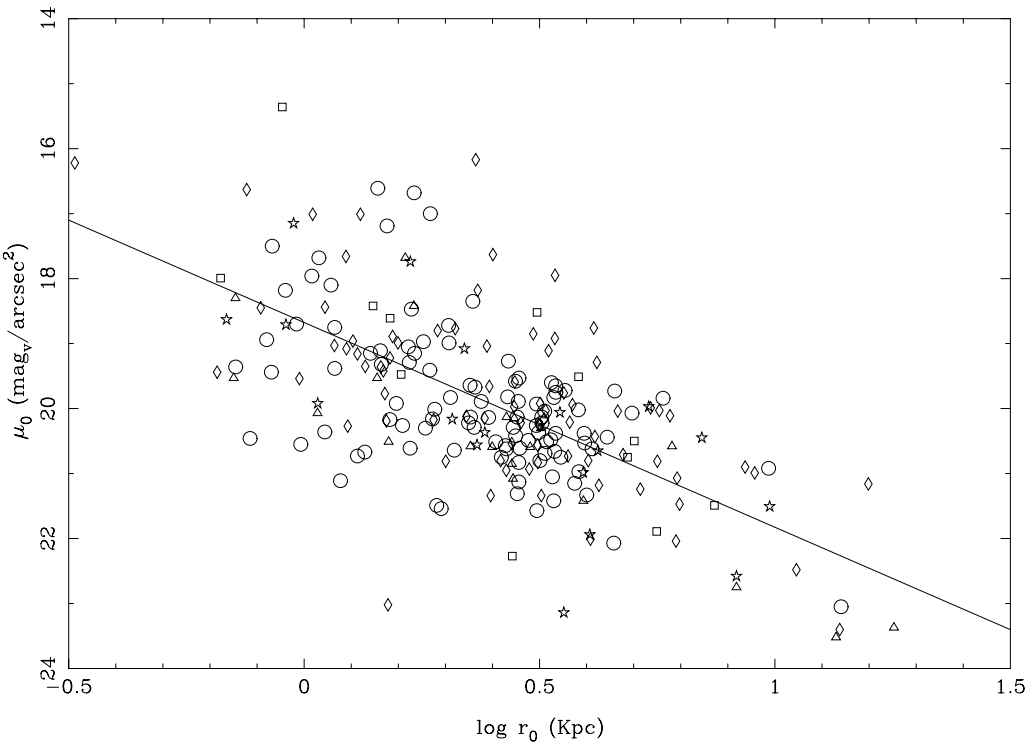

Figure 4. Disc parameters μ_0 and log r_0 (mag arcsec^{-2}, radii in kpc). Seyfert 1 galaxies are represented as stars, Seyfert 2 galaxies as squares, LINERs as diamonds, starbursts as open circles and normal galaxies as triangles. The solid line shown is the result of a linear regression. A weak linear correlation is observed (the correlation coefficient is only about 0.65).

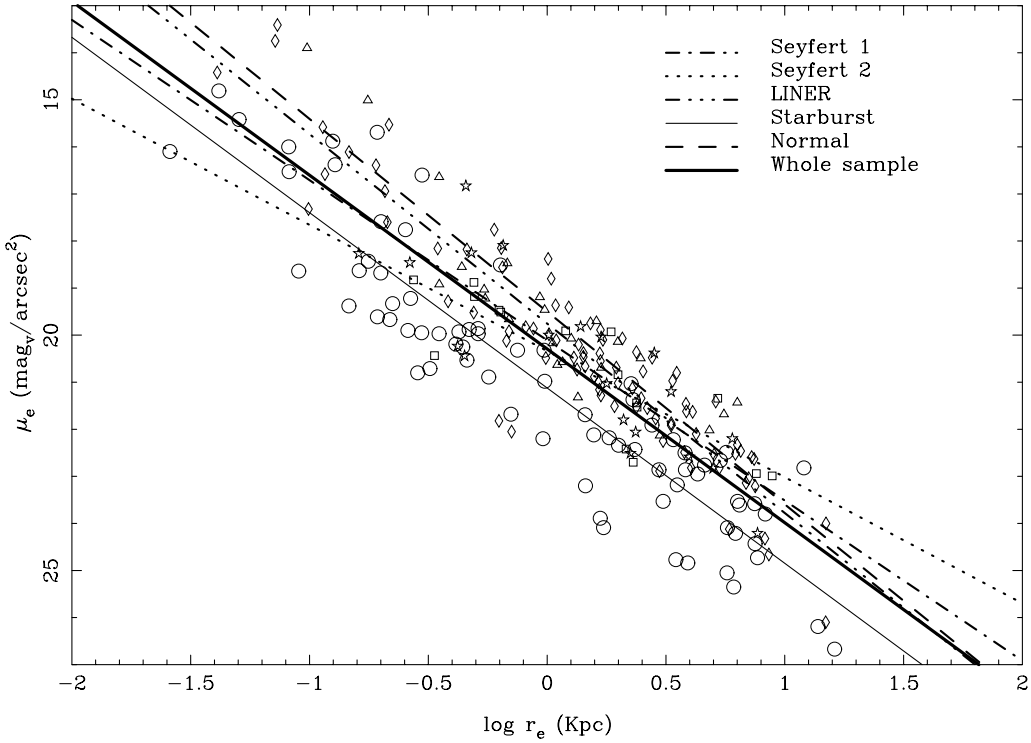

Figure 5. Bulge parameters μ_e and log r_e (mag arcsec^{-2}, radii in kpc). Symbols as in Fig. 4. Regression lines have been plotted for all nuclear types.

(iv) From $T = 1$ onwards, $(B/D)_{\rm median}$ is quite uniform across all nuclear types.

5.2 Radial colour distribution

Yee (1983) performed Gunn *r*, *g*, *v* surface photometry on a sample of 20 Seyfert galaxies from the Markarian catalogue concluding that the colours of the underlying galaxies are comparable to those of normal spirals in the Sa–Sbc range, but the nuclear colours are bluer in Seyfert 1 galaxies than in Seyfert 2 objects. Xanthopoulos (1996) performed aperture photometry on a sample of 27 Seyfert 1 and Seyfert 2 galaxies using 2.5, 5, 10 and 20 kpc apertures. No differences (within the measurement uncertainties) were found in the $V - R$, $R - I$ and $V - I$ colours in the 10-kpc and 20-kpc apertures characterizing the disc. In the 2.5-kpc and 5-kpc apertures, however, the $R - I$, and, to a lower degree, the $V - I$ colours appear bluer in Seyfert 1 galaxies than in Seyfert 2.

It should be taken into account that AGN aperture photometry is contaminated by nuclear emission lines and it is expected that this effect would be more noticeable in the smaller diaphragms. This is specially true for the $R - I$ colour in Seyfert 1 galaxies, since the *R*-band contains the broad component of Hα. $R - I$ colours are then expected to be bluer in Seyfert 1 galaxies than in Seyfert 2 galaxies. Since we are interested in characterizing the underlying galaxy colours, we would need to parametrize them avoiding the nuclear emission lines. To this end, we have used the radial colour

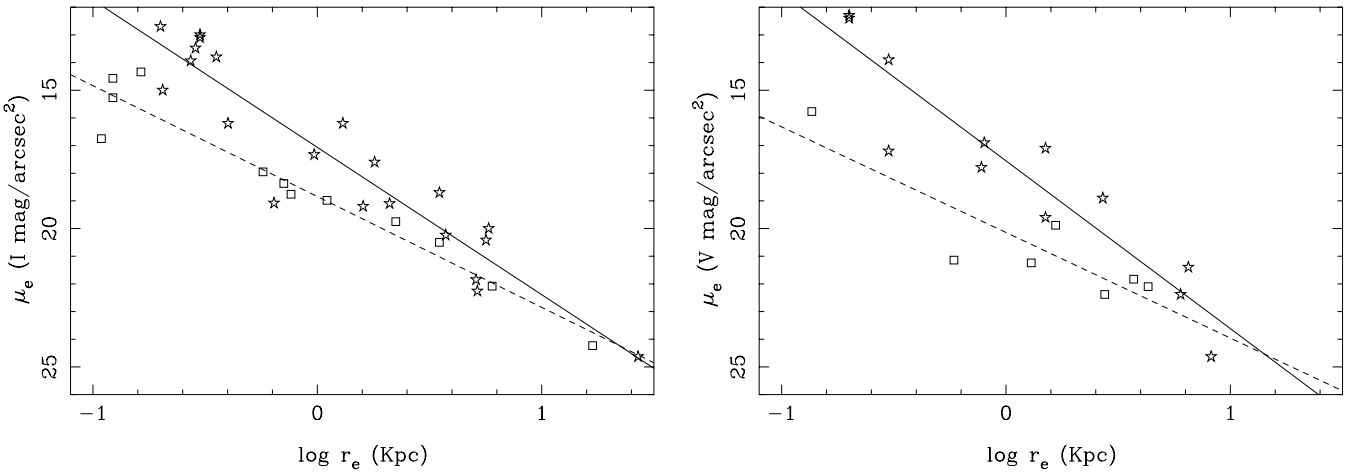

Figure 6. Bulge parameters μ_e and log r_e (mag arcsec^{-2}, radii in kpc) for the comparison sample in the *I* (left) and *V* bands. Symbols as in Fig. 4. The solid line corresponds to the linear regression for Seyfert 1 galaxies and the dashed line to Seyfert 2 galaxies. Differences in the slope of both distributions are $\simeq$2.4 σ in the *I* band and $\simeq$1.9 σ in the *V*-band.

Table 5. Type II discs versus nuclear type.

Nuclear type	No. of objects with disc fit	No. of objects with type II disc	Ratio (per cent)
Seyfert 1	19	6	31.6
Seyfert 2	12	4	33.3
LINER	80	31	38.7
Starburst	103	24	23.3
Normal	20	8	40.0

Table 6. Type II discs versus Hubble type.

Hubble type T	No. of objects with disc fit	No. of objets with type II disc	Ratio (per cent)
−3	11	6	54.5
−2	21	9	42.9
−1	21	11	52.4
0	12	6	50.0
1	16	3	18.7
2	19	3	15.8
3	25	7	28.0
4	38	10	26.3
5	41	14	34.1
6	19	4	21.0

Table 7. Median B/D relation versus morphological type. SDV mean B/D values are shown for comparison.

Hubble type T	No. of objets	$(B/D)_{\rm median}$	mean dev.	$\langle B/D \rangle$ (SDV)	mean dev. (SDV)
−3	11	1.44	0.52	1.43	0.42
−2	21	1.89	1.29	1.33	0.24
−1	20	2.06	1.23	1.27	0.32
0	12	1.58	1.27	1.02	0.13
1	16	0.66	0.45	0.55	0.32
2	18	0.49	0.36	0.48	0.10
3	20	0.76	0.38	0.29	0.05
4	33	0.25	0.19	0.22	0.06
5	29	0.40	0.29	0.11	0.02
6	10	0.18	0.22	0.04	0.01
7	2	0.49	0.22	0.02	0.01
8	–	–	–	–	–
9	2	0.10	0.003	–	–

distributions presented in Paper I, analysing the $R - I$ and $V - I$ colour profiles. While radial distributions of bulges and discs generally become bluer outward (Balcells & Peletier 1994), gradients are small enough that it is possible to assign representative values for the colour of each component. For instance, Peletier & Balcells (1996) selected as characteristic of bulges the colour at $0.5 \times r_{\rm e}$ or at 5 arcsec, whichever is larger, and for discs the colours at $2 \times r_0$.

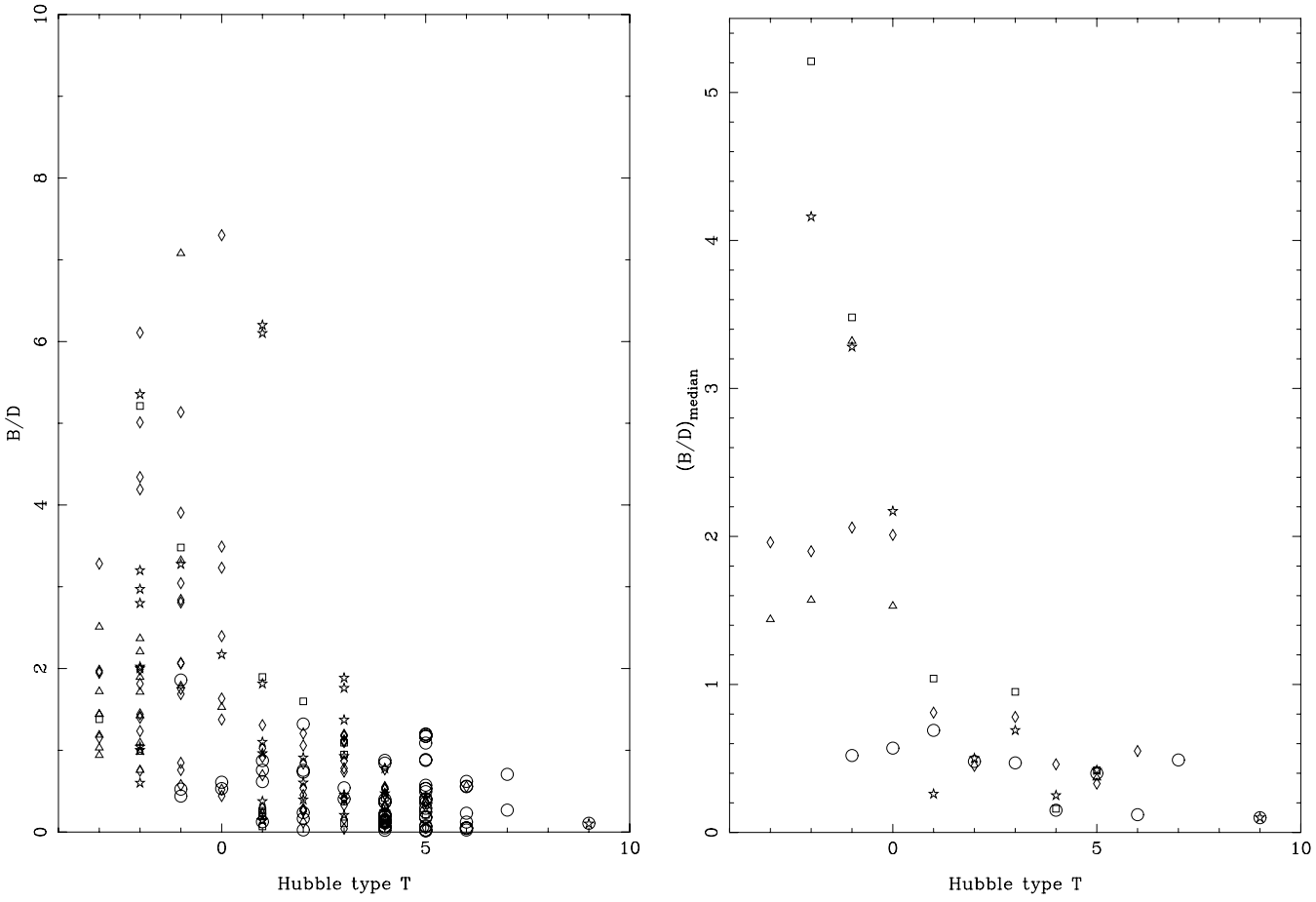

Figure 7. Distribution of the B/D relation (left panel) and median value $(B/D)_{\rm median}$ (right panel) for the different morphological types. Symbols as in Fig. 4.

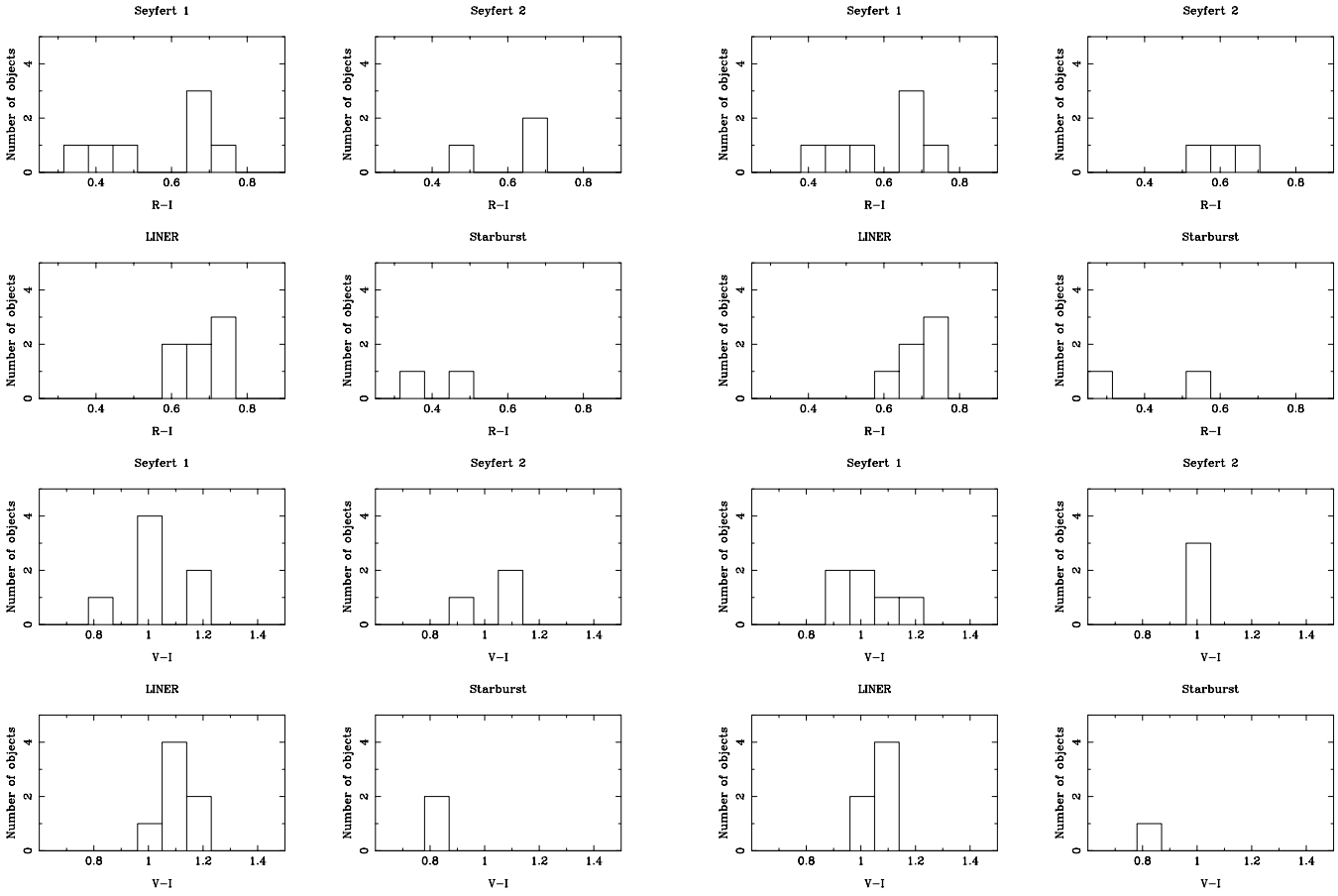

Figure 8. Distribution of bulge (left) and disc characteristic colours.

In order to minimize the risk of nuclear contamination at small radii in bulges and too high colour errors at large radial distances in discs, we have decided to select as representative the colours at effective radius (r_e) for bulges and those at scalelength (r_0) for discs.

The results are somewhat qualitative, since statistics are not reliable for such a small sample. As shown in Fig. 8, we have found that the range of characteristic bulge and disc colours is comparable in all nuclear types, albeit mean bulge and disc characteristic colours are bluer in Seyfert galaxies than in LINERs. Seyfert 1 bulge and disc characteristic colours are somewhat bluer than those of Seyfert 2. Nevertheless, it should be taken into account that the bluest Seyfert 1 observed bulge colours are almost certainly contaminated by either the NLR component (NGC 3227) or by circumnuclear star-forming rings (NGC 3982 and NGC 7469).

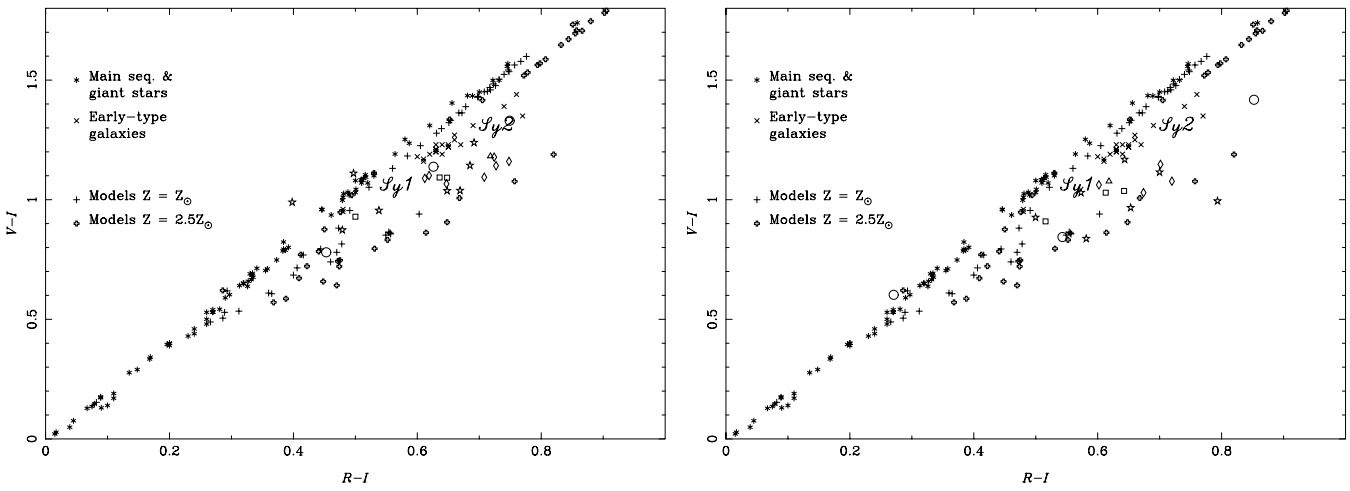

Figure 9. Bulge (left) and disc (right) characteristic colours compared with photoelectric photometry of stars and early-type galaxies and with population synthesis-derived colours. Symbols as in Fig. 4. The points labelled as *Sy1* and *Sy2* correspond to the mean Seyfert 1 and Seyfert 2 colours in the 5-kpc aperture from Xanthopoulos (1996).

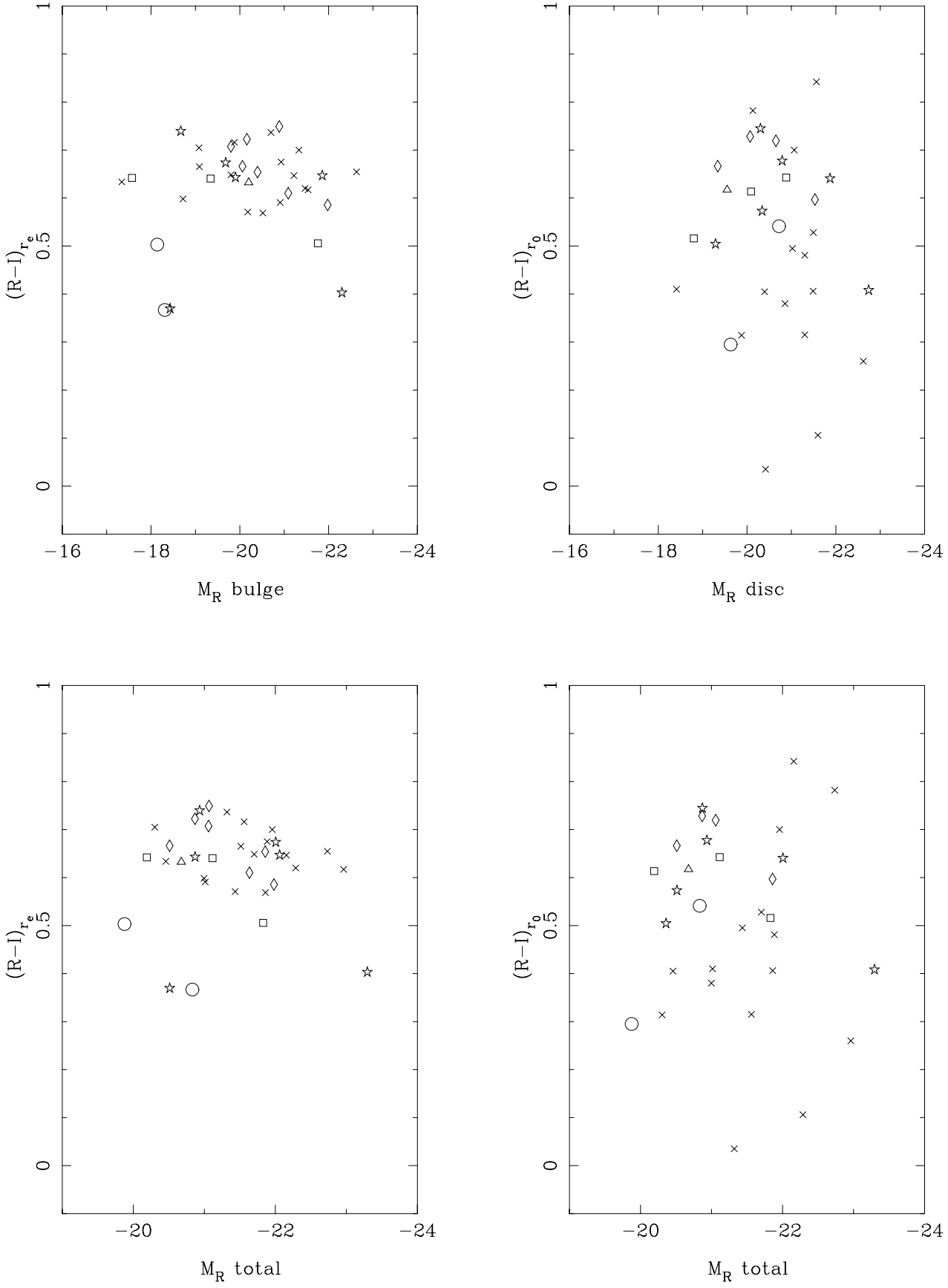

Figure 10. Sample bulge (left diagrams) and disc (right diagrams) characteristic colours (symbols as in Fig. 4) plotted against bulge, disc and total absolute magnitudes. The comparison sample (crosses) comprises 18 early-type galaxies from Balcells & Peletier (1994) and Peletier & Balcells (1996).

As a first comparison, we have represented in Fig. 9 our bulge and disc colours along with photoelectric photometry values of standard stars from Moreno & Carrasco (1986) and Graham (1982) and aperture photometry of early-type galaxies from Poulain (1988). We have also included colours from population synthesis models computed by Bressan, Chiosi & Fagotto (1994) at $Z = Z_{\odot}$ and $Z = 2.5\,Z_{\odot}$ and a large range of ages (from 6.3×10^6 to 19.95×10^9 yr). There is an acceptable agreement between our colours and those of the comparison sample: they are comprised between those derived from aperture photometry of early-type galaxies (whose colours are generally redder) and the population-synthesis models.

A further step is the comparison of our characteristic colours with those of normal galaxies with similar morphological type. To this end, we have selected a reference sample of 18 early-type galaxies (Balcells & Peletier (1994); Peletier & Balcells (1996); these studies will be referenced hereafter as BP). Three of them are catalogued as normal galaxies in HFS, while four of the galaxies have been labelled as transition types or LINERs. The remaining 11 objets are not included in the HFS sample, but have been checked in the NASA/IPAC Extragalactic Database (NED) and in Véron-Cetty & Véron (2000) for the absence of active nucleus.

Characteristic colours from BP have been derived from colour gradients rather than from the colour profiles themselves. These authors find that bulge colours are predominantly bluer than those of elliptical galaxies, but both bulges and ellipticals follow the same sequence in the colour–colour diagram. They conclude that stellar populations of bulges must be similar to those of elliptical galaxies, but the former, as a class, have lower metallicities and larger spread in ages than giant ellipticals. Visvanathan & Sandage (1977) found that ellipticals and S0 galaxies follow a colour–magnitude relation in which brighter galaxies are redder; BP also tried to correlate bulge colours and global galaxy parameters. They find that the (weak) correlation between colours and absolute magnitude improves slightly when the total galaxy luminosity is used instead of the bulge luminosity alone. This might indicate that the total galaxy potential, and not the bulge alone, determines the chemical enrichment of the bulge. Moreover, they find that bulge and disc colours derived from profiles are very similar, suggesting that the bulk of the inner disc and bulge stars are essentially coeval. At most, disc stars are 2–3 Gyr younger than bulge stars.

Fig. 10 shows the relationship between our characteristic $R - I$ colours and the bulge, disc and total galaxy luminosity. BP data have also been plotted in order to compare the control sample colours with ours. We find that:

(i) When comparing our sample with the control sample, we find a very similar colour range; this is true for both bulge and disc components and may suggest that the bulge and disc stellar populations (ages and metallicities) are comparable in normal and active galaxies.

(ii) We confirm the result from BP that bulges and disc characteristic colours derived from profiles are very similar, though there is a wider range of disc characteristic colours.

(iii) We are not able to confirm a correlation between bulge colours and bulge luminosity. Moreover, this situation does not improve when using the total galaxy luminosity instead of the bulge luminosity alone.

6 CONCLUSIONS

We have investigated the main structural properties derived from *VRI* and Hα surface photometry of galaxies hosting nuclear emission-line regions (including Seyfert 1, Seyfert 2, LINER and starburst galaxies) as compared with normal galaxies. Our original sample is thoroughly described in Paper I and comprises 21 active galaxies, three starbursts and one normal galaxy. For our investigation on bulge and disc parameter distributions, we have extended the sample up to 261 objects hosting all levels of nuclear activity (ranging from normal to Seyfert 1 galaxies). Our study has found several differences between the structural parameters of active and non-active galaxies. From the statistical analysis performed in Section 5.1.2, we cannot claim that the individual morphological parameters of active and non-active galaxies follow the same statistical distribution. On the other hand, we have studied the distribution of morphological parameters in the (μ_0, log r_0) and (μ_e, log r_e) planes. Disc parameters are found strongly clustered (perhaps a selection effect) but the linear correlation is weak. On the other hand, there is a strong linear correlation of bulge parameters. We have studied the distributions across the different nuclear types, finding that starbursts constitute a lower luminosity bulge class. LINERs and normal galaxies follow very similar distributions. Seyfert 1, Seyfert 2 and LINERs follow different distributions at statistically significant level. These differences could perhaps imply families of bulges with different physical properties. Type II discs are analysed in Section 5.1.3. We do not find a correlation between type II discs and nuclear type but do with Hubble type. The B/D relation is studied in Section 5.1.4. We find that the distribution of $(B/D)_{\rm median}$ seems to be generally independent of the nuclear type, except for the earliest ($T < 0$) Hubble types. Finally, bulge and disc characteristic colours derived from radial profiles have been investigated in Section 5.2. We find that the range of characteristic bulge and disc colours is comparable in all nuclear types, though mean bulge and disc colours are bluer in Seyfert galaxies than in LINERs. Nevertheless, this result is uncertain since bulge colours can be affected by line emission contamination arising from the NLR and/or circumnuclear star-forming regions. When comparing our characteristic bulge and disc colours with those of the control sample of early-type galaxies,we find a very similar colour range that may suggest that the bulge and disc stellar populations are comparable in normal and active galaxies. On the other hand, we find that bulges and disc characteristic colours derived from profiles are very similar. We do not detect a correlation between bulge colours and bulge or total galaxy luminosities.

ACKNOWLEDGMENTS

The JKT is operated on the island of La Palma by the Isaac Newton Group in the Spanish Observatorio del Roque de los Muchachos of the Instituto de Astrofísica de Canarias. We would like to thank CAT for awarding observing time. We also thank an anonymous referee for suggestions that greatly improved the clarity of the paper. This research has made use of the NASA/IPAC Extragalactic Database (NED) which is operated by the Jet Propulsion Laboratory, California Institute of Technology, under contract with the National Aeronautics and Space Administration. MS-P would like to thank Isabel Casanova for her assistance entering and revising the large amount of data from the literature. This work has been partially supported by DGICYT project AYA-2000-0973.

REFERENCES

Adams T. F., 1977, ApJS, 33, 19
Andredakis Y. C., Peletier R. F., Balcells M., 1995, MNRAS, 275, 874
Baggett W. E., Baggett S. M., Anderson K. S. J., 1998, AJ, 116, 1626

Balcells M., Peletier R. F., 1994, AJ, 107, 135
Boris N. V., Donzelli C. J., Pastoriza M. G., Rodríguez-Ardila A., Ferreiro D. L., 2002, A&A, 348, 780
Boroson T., 1981, ApJS, 46, 177
Bressan A., Chiosi C., Fagotto F., 1994, ApJS, 94, 63
Capaccioli M., de Vaucouleurs G., 1983, ApJS, 52, 465
Capaccioli M., Caon N., D'Onofrio M., 1992, MNRAS, 259, 323
Carollo C. M., Stiavelli M., Mack J., 1998, AJ, 116, 68
Carone T. E., 1992, in Filippenko A. V. ed., ASP Conf. Ser. Vol. 31, Relationships between Active Galactic Nuclei and Starburst Galaxies. Astron. Soc. Pac., San Francisco, 375
de Jong R. S., 1996, A&AS, 118, 557
de Vaucouleurs G., de Vaucouleurs A., Corwin H. G. Jr, Buta R., Paturel G., Fouqué P., 1991, Third Reference Catalog of Bright Galaxies, New York, Springer (RC3)
de Vaucouleurs G., 1948, Ann. d'Astrophys., 11, 247
Díaz A. I., Álvarez Álvarez M., Terlevich E., Terlevich R., Sánchez-Portal M., Aretxaga I., 2000, MNRAS, 311, 120
Ferrarese L., Pogge R. W., Peterson B. M, Merritt D., Wandel A., Joseph C. L., 2001, ApJ, 555, L79
Freeman K. C., 1970, ApJ, 160, 811
Freeman K. C., 1976, in Proc. Sixth Advanced Course, Saas-Fee, Switzerland. Obser. de Genève, Sauverny
Graham J. A., 1982, PASP, 94, 244
Ho L. C., Filippenko A. V., Sargent W. L. W., 1997, ApJS, 112, 315 (HFS)
Hoessel J. G., Oegerle W. R., Schneider D. P., 1987, AJ, 94, 1111
Hunt L. K., Giovanardi C., 1992, AJ, 104, 1018
Hunt L. K., Malkan M. A., Salvati M., Mandolesi N., Palazzi E., Wade R., 1997, ApJS, 108, 229
Hunt L. K., Malkan M. A., Moriondo G., Salvati M., 1999, ApJ, 510, 637
Jiménez-Benito L., Díaz A. I., Terlevich R. J., Terlevich E., 2000, MNRAS, 317, 907
Kent S. M., 1985, ApJS, 59, 115
Kodaira K., Okamura S., Ichikawa S., 1990, Photometric Atlas of Northern Bright Galaxies. Univ. Tokyo Press, Tokyo
Kormendy J., 1977, ApJ, 217, 406
Kormendy J., 1983, in Proc. Twelfth Advanced Course, Saas-Fee, Switzerland. Obser. de Genève, Sauverny
MacKenty J. W., 1990, ApJS, 72, 231
Márquez I, Moles M., 1994, AJ, 108, 90
Márquez I. et al., 1999, A&AS, 140, 1
Márquez I. et al., 2000, A&A, 360, 431
Mediavilla E., Pastoriza M. G., Battaner E., 1989, Ap&SS, 157, 145
Moreno H., Carrasco G., 1986, A&AS, 65, 33
Mulchaey J. S., Regan M. W., 1997, ApJ, 482, L135
Nelson C. H., Whittle M., 1996, ApJ, 465, 96
Pastoriza M. G., Mediavilla E., Battaner E., 1989, in Osterbrok D. E., Miller J. S., eds, IAU Symposium 134, Active Galactic Nuclei. Kluwer, Dordrecht
Peletier R. F., Balcells M., 1996, AJ, 111, 2238
Poulain P., 1988, A&AS, 72, 215
Sánchez-Portal M., Díaz A. I., Terlevich R., Terlevich E., Álvarez Álvarez M., Aretxaga I., 2000, MNRAS, 312, 2 (Paper I)
Schombert J. M., Bothum G. D., 1987, AJ, 92, 60
Sérsic J. L., 1968, Atlas de Galaxias Australes. Observatorio Astronómico, Córdoba
Shlosman I., Begelman M., Frank J., 1989, Nat, 338, 45
Simien F., de Vaucouleurs G., 1986, ApJ, 302, 564 (SDV)
Terlevich E., Díaz A. I., Terlevich R. J., 1990, MNRAS, 242, 271
Terlevich R. J., Sánchez-Portal M., Díaz A. I., Terlevich E., 1991, MNRAS, 249, 36
Véron-Cetty M.-P., Véron P., 1993, A Catalogue of Quasars and Active Nuclei;, 6th edn.
Véron-Cetty M.-P., Véron P., 2000, A Catalogue of Quasars and Active Nuclei;, 9th edn.
Virani S. N., De Robertis M. M., VanDalfsen M. L., 2000, AJ, 120, 1739
Visvanathan N., Sandage A., 1977, ApJ, 216, 214
Xanthopoulos E., 1996, MNRAS, 280, 6
Yee H. K. C., 1983, ApJ, 272, 473

This paper has been typeset from a TEX/LATEX file prepared by the author.